ELSEVIER

Progress in Nuclear Magnetic Resonance Spectroscopy 43 (2003) 63–103

PROGRESS IN NUCLEAR MAGNETIC RESONANCE SPECTROSCOPY

www.elsevier.com/locate/pnmrs

Chemical exchange in NMR

Alex D. Bain*

Department of Chemistry, McMaster University, 1280 Main St West, Hamilton, Ont., Canada L8S 4M1

Received 3 June 2003

Contents

Keywords: Dynamic NHR; Chemical exchange; Fluxionality; Lioville space; Transition probabilities; Density matrix; Kinetics; Data fitting

1. Introduction

Almost everyone who has done NMR has seen some evidence of chemical exchange. This could be the classic line broadening and coalescence phenomenon (Fig. 1), the lack of coupling to hydroxide protons, cross-peaks in a NOESY-type spectrum or several other observations. The ways that chemical exchange affects NMR spectra are very diverse, but the basic mechanism is much the same. In this review, we will stress the underlying similarities in the broad range of experimental manifestations. We will concentrate on liquid-state NMR, since this is the simplest and most familiar subject. However, exchange also happens in the gas phase and in the solid state. Particularly in solids, there is a richness of the interactions that leads to many unusual effects. However, all these effects have a common basis.

* Fax: +1-905-522-2509.
E-mail address: bain@mcmaster.ca (A.D. Bain).

doi:10.1016/j.pnmrs.2003.08.001

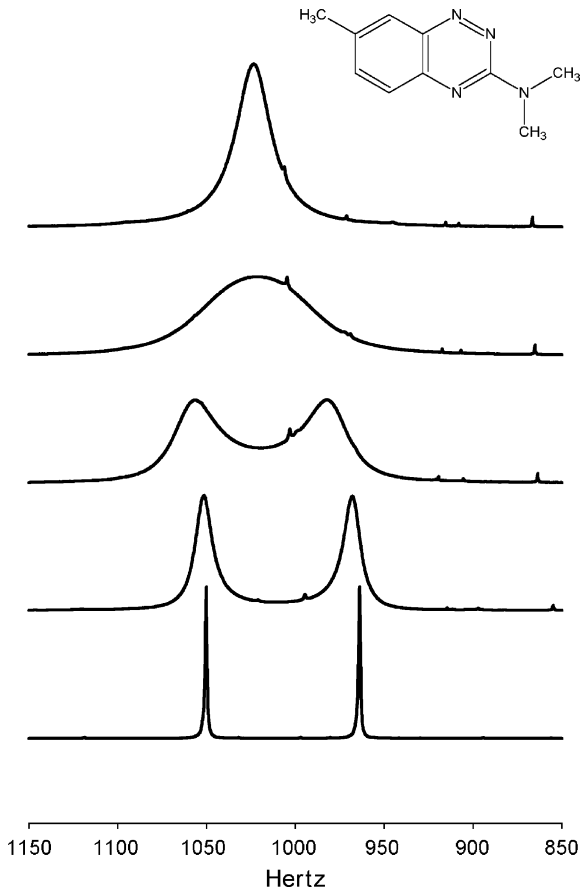

Fig. 1. Proton NMR spectra at 300 MHz of the *N*-methyl signals in a derivative of azapropazone (structure shown in the figure) [225] as a function of temperature. The lowest spectrum is at 223 K, and then at 243, 253, 263, and 273 K.

Nuclei with spin resonate at a characteristic frequency when placed in a magnetic field, hence NMR spectroscopy. In the simplest case, an isolated spin-1/2, this will give rise to a single, extremely sharp resonance. The resonance position is exquisitely sensitive to the magnetic environment—one of the reasons why NMR is so useful. Since we routinely resolve resonances that differ by fractions of a part per million (ppm), many fine details of the chemical environment of the nucleus are revealed.

If some dynamic process takes a given nucleus from one magnetic environment to a different one, the NMR spectrum will be affected. The effects can be dramatic, if the rate of the exchange is in an appropriate range (Fig. 1). We keep the definitions of a process and a magnetic environment deliberately vague, since similar NMR phenomenons occur in many different physical and chemical situations. The observed effects of the dynamic processes are quite different, depending on the system and the process. The effects may be obvious or very subtle, but they are present in many NMR spectra.

Normally, the spectra are measured in macroscopic equilibrium—the sample is (we hope) not changing as we acquire the NMR spectrum. Therefore, the process is often referred to as chemical exchange. When an individual nucleus moves to a different environment, it is always replaced, maintaining the equilibrium. On the lab scale, the sample shows no signs of reaction—the chemical exchange only becomes evident in the NMR spectrum. The evidence of exchange will change from situation to situation, but the principles are always the same.

The study of chemical exchange is a classic part of NMR spectroscopy [1,2], and there are several excellent books and standard reviews [3–12]. In particular, the book edited by Jackman and Cotton [3] is an essentially complete review of the field up until the early 1970s and covers most of the fundamentals. We find Sandstrom's book [4] a very readable introduction, if somewhat dated in parts. Much has happened since the publication of these books (see the more recent compilations [6,7,13]), but the older books still provide a good start. The aim of this review is to attempt an overview of exchange effects in many branches of NMR. It certainly cannot be exhaustive, but we hope it is representative.

Figs. 1–7 show some examples of the variety of chemical exchange effects. The classic exchange between two equally populated sites is shown in Fig. 1. As with Gutowsky's work on dimethylamides and many other studies [14], it shows the spectrum of an *N*,*N*-dimethylgroup bonded to a π system [15]. These systems form the prototype for illustrating chemical exchange effects. Fig. 2 shows some lineshapes for *para*-nitrosodimethylaniline [16,17]. Now the spins show scalar coupling. In this case, the nitroso group lies in the plane of the ring, but it can flip from one side to the other. The four aromatic protons are all magnetically distinct,

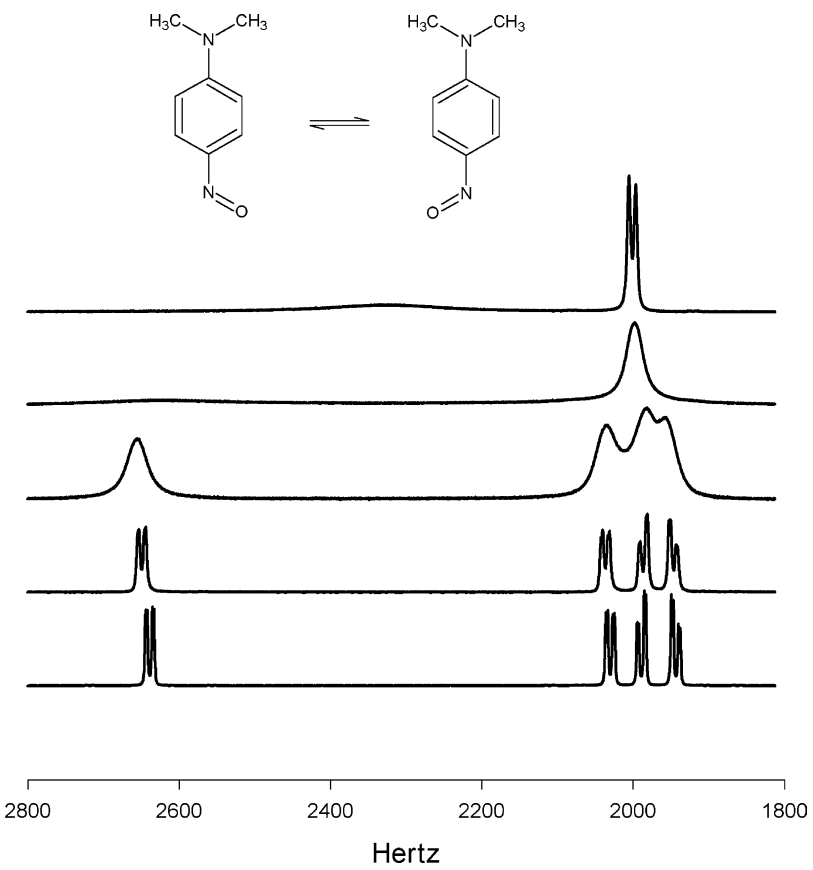

Fig. 2. Proton NMR spectra at 400 MHz of the aromatic protons in *p*-nitrosodimethylaniline (structure shown in figure), as a function of temperature. The nitroso group exchanges from one side of the aromatic ring to the other. The spectra were run at 213, 243, 263, 283 and 303 K, starting from the bottom spectrum.

but when the nitroso group flips to the other side, the chemical shifts and couplings are swapped. All the lines are broadened, since the magnetic environments are all different. This is a case of mutual exchange, in which the molecule is identical in both sites. In Fig. 3, the three aromatic protons of a diacylpyridine group in a metal complex [18] are shown. In this complex, only one of the acyl groups bonds to the metal, rendering the ligand asymmetric. However, the metal can jump to the other acyl group, creating the exchange process. The central proton in the diacylpyridine ring has the same environment regardless of which acyl group is bonded to the metal. Its signal remains as a sharp pseudo-triplet regardless of the rate, but the other signals broaden as in the previous case. Fig. 4 shows an intermolecular exchange in an equilibrium between a monomeric and dimeric metal complex [19]. The figure shows the methyl signals of the trimethylphosphine group, with the coupling to ^{31}P; the signals at higher frequency correspond to the monomer. This is a non-mutual exchange, since the two sites (monomer and dimer) are chemically different. Also, the populations of the two sites are different. However, the coupling to the phosphorus is always maintained, so the doublet splitting is observable in all the spectra. Fig. 5 shows the proton spectrum of an ethanol–water mixture, as a function of temperature [20]. At low temperature, the water and the alcohol OH have separate signals, and the OH shows a vicinal coupling to the methylene protons. At higher temperature,

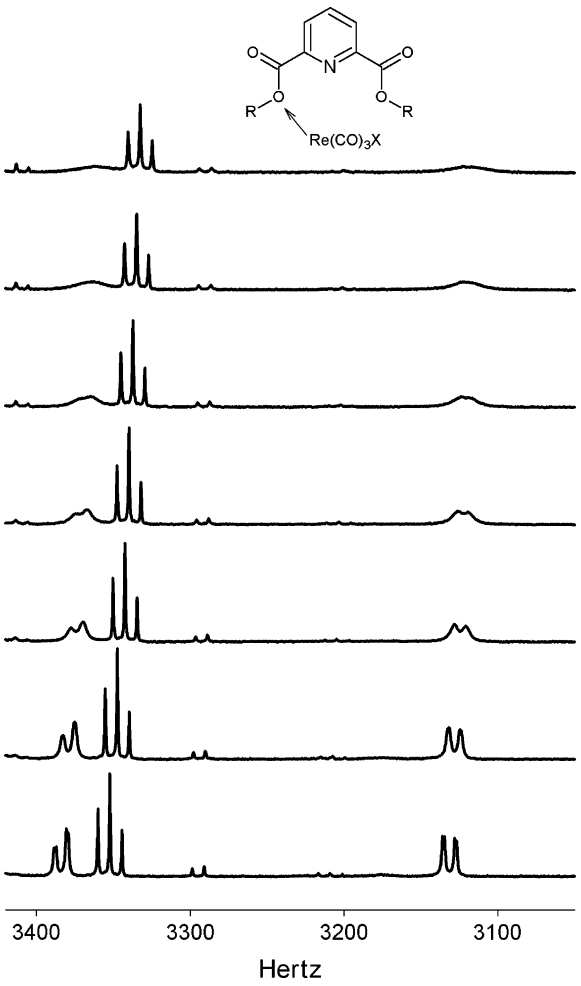

Fig. 3. Proton NMR spectra at 300 MHz of the aromatic protons in a rhenium complex of diacylpyridine (structure shown in figure), as a function of temperature [18]. The Re atom bonds to one of the acyl groups, rendering the protons inequivalent, but the metal can exchange between acyl groups. The middle proton signal remains sharp, since its parameters are not affected by the exchange. We are grateful to Dr Keith Orrell and Dr Vladimir Sik for providing us with this set of data.

the methylene protons have lost the coupling to the OH, and the water and the OH signals are starting to merge. The rate of exchange of water protons with OH and NH protons is widely variable, depending on concentration and pH, so separate signals may or may not be observed.

These examples show several of the sub-classifications of chemical exchange: coupled vs. uncoupled spin systems, mutual vs. non-mutual exchange, intermolecular vs. intramolecular reactions. After we have described the theory behind these lineshapes and other effects, we will return to examine these examples in more detail.

The lineshape is the most obvious manifestation of chemical exchange, and there is a tendency to treat it differently from 'normal' NMR spectra. A spectrum with no dynamics is usually considered as a sum of individual transitions, whereas a dynamic spectrum is formulated as a unitary lineshape. One of the aims of this review is to break down this distinction. With a simple extension of the idea of a transition probability, we can also treat dynamic lineshapes as a sum of transitions.

These are all one-dimensional (1D) spectra. Multi-dimensional spectra require pulse sequences, and the coherence must remain long enough to be transferred by the pulses. Unfortunately, the incoherent process of chemical exchange usually makes T_2 too short to be useful [21,22]. However, intramolecular chemical exchange affects chemical shifts more than couplings, so coherence transfer may be surprisingly efficient in proton–carbon correlation experiments [23]. In this particular molecule, the proton lines are sharp, but the carbon is in intermediate exchange. The broad lines are very weak in the 1D carbon spectrum, but quite sharp in the two-dimensional (2D) HMQC spectrum. Slower chemical exchange, on the timescale of the pulse sequence can produce effects in most pulse sequences, such as DOSY [24] and TOCSY [25,26].

If the exchange happens on the relatively slow timescale of spin–lattice relaxation, then the effects on the lineshape are not obvious. However, relaxation experiments can be strongly affected [27]. If one of the exchanging sites is selectively inverted, and the z magnetizations measured after a series of suitable delays, we get a series of spectra as in Fig. 6. These are experiments on dimethylacetamide, in which the signal of one of the methyl groups on the nitrogen was inverted. The spins that were inverted can regain their equilibrium state by both spin relaxation and chemical exchange with the non-inverted site. When an exchange process happens, it swaps an inverted spin for a non-inverted spin. This means that the inverted site

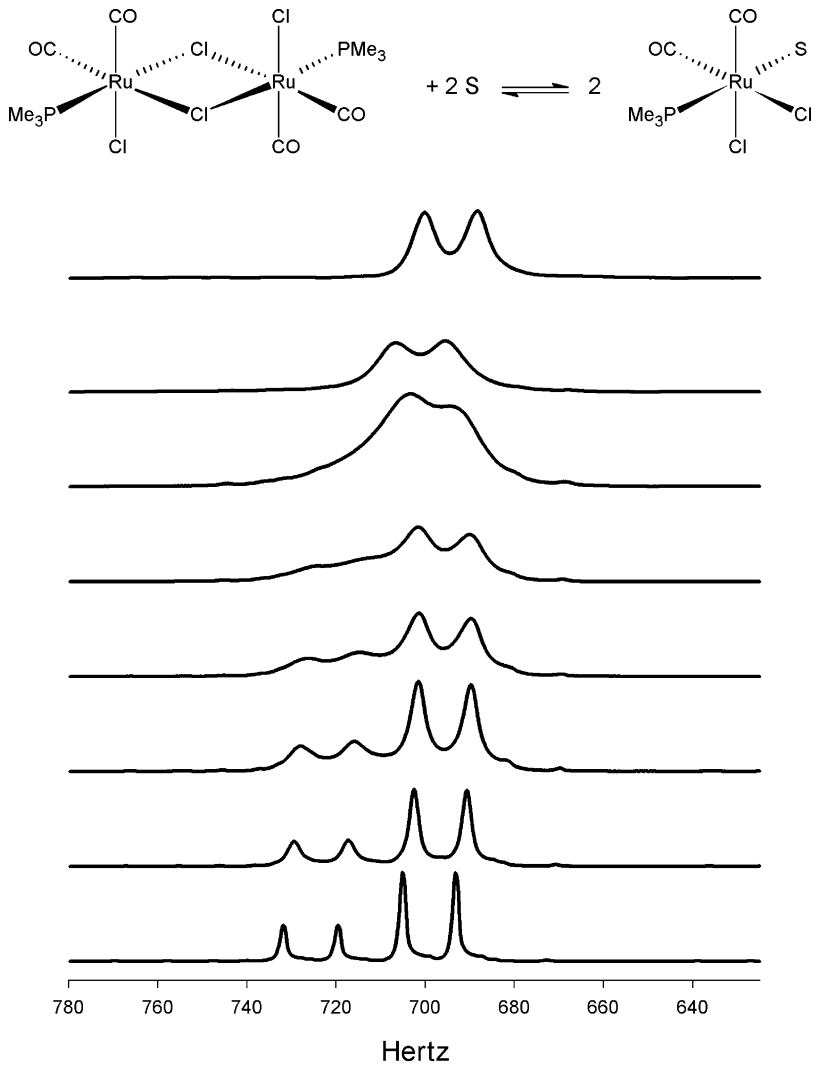

Fig. 4. The methyl region of the proton spectrum at 400 MHz of a solution of $Ru_2(\mu\text{-}Cl)_2Cl_2(CO)_4(PMe_3)_2$ in dmf-d_7. The dimeric molecule exists in equilibrium with a monomeric form (the signals at high frequency). Throughout the exchange, the coupling to phosphorus is maintained. We are grateful to Dr Marcel Schlaf for this data.

relaxes more quickly than the rate determined by T_1, and the non-inverted signal has a transient decrease in intensity before relaxing back to equilibrium. This experiment gives excellent data for quantitative measurement of exchange rates. The same physical mechanism underlies the 2D EXSY experiment (analogous to NOESY) [28], in which cross-peaks indicate the presence of exchange between sites (Fig. 7). At short mixing times, the cross-peak is very small, but it becomes significant as the mixing time is increased. Cross-peaks in an EXSY spectrum are a very useful qualitative indicator of the presence of slow chemical exchange.

When the exchange is fast, the spectrum consists of a single peak, slightly broadened by the exchange process, as in Fig. 8. In this molecule, the two acyl groups on the glycoluril framework [29] are asymmetric, but can exchange. The methyls on the bridgehead carbons are unaffected by the exchange, but the methyls on the nitrogens show

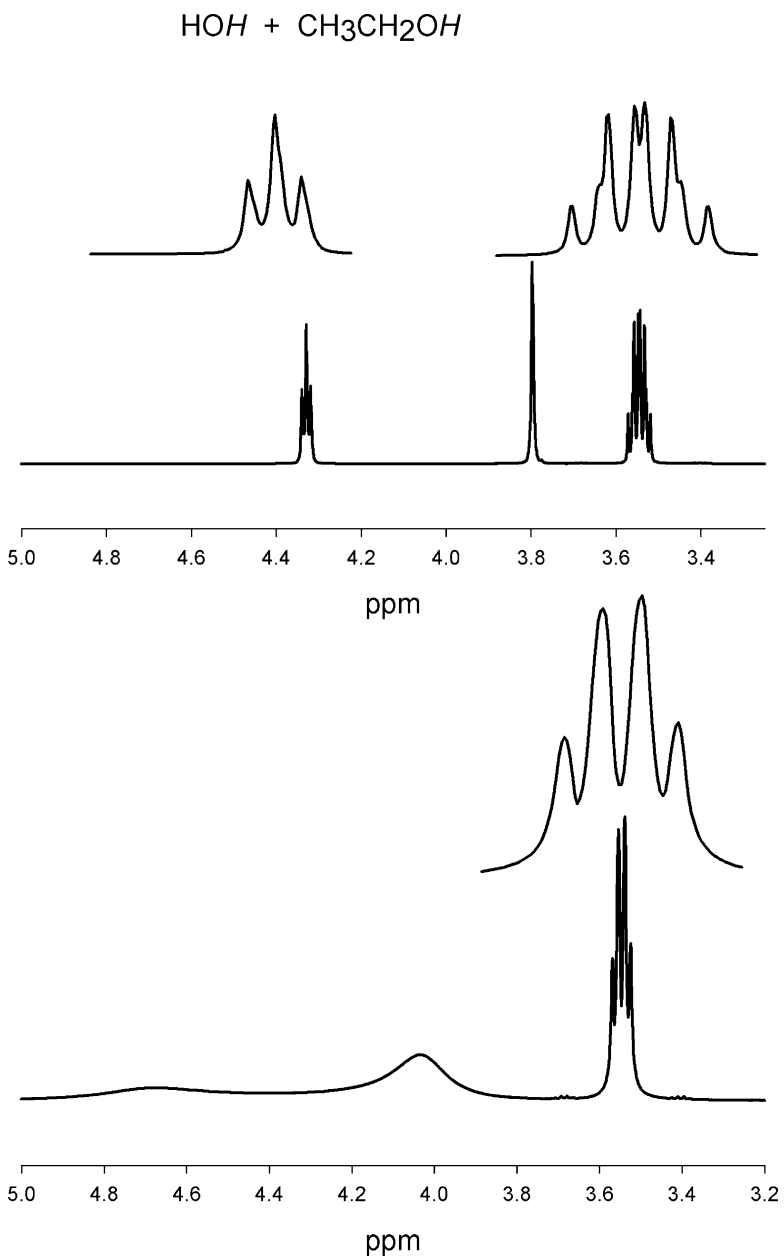

Fig. 5. Proton NMR spectra at 500 MHz of a mixture of ethanol and water, in acetone-d_6. The top spectrum is at 253 K, and the expansions show the coupling between the OH proton at 4.35 ppm and the CH_2 protons at 3.55 ppm. The signal at 3.8 ppm is due to the water. The bottom spectrum is at 333 K, and show the loss of coupling in the CH_2 group and the start of coalescence of the ethanol OH proton and the water peak.

separate signals at low temperatures. After coalescence, as the temperature is increased, the *N*-methyl signal gets sharper and sharper. The line broadening is evidence of a short T_2, the spin–spin relaxation time. If we measure T_2 using the Carr–Purcell–Meiboom–Gill (CPMG) spin echo sequence, we see the decay, but we may also see that the apparent T_2 depends on the timescale of the refocussing pulses

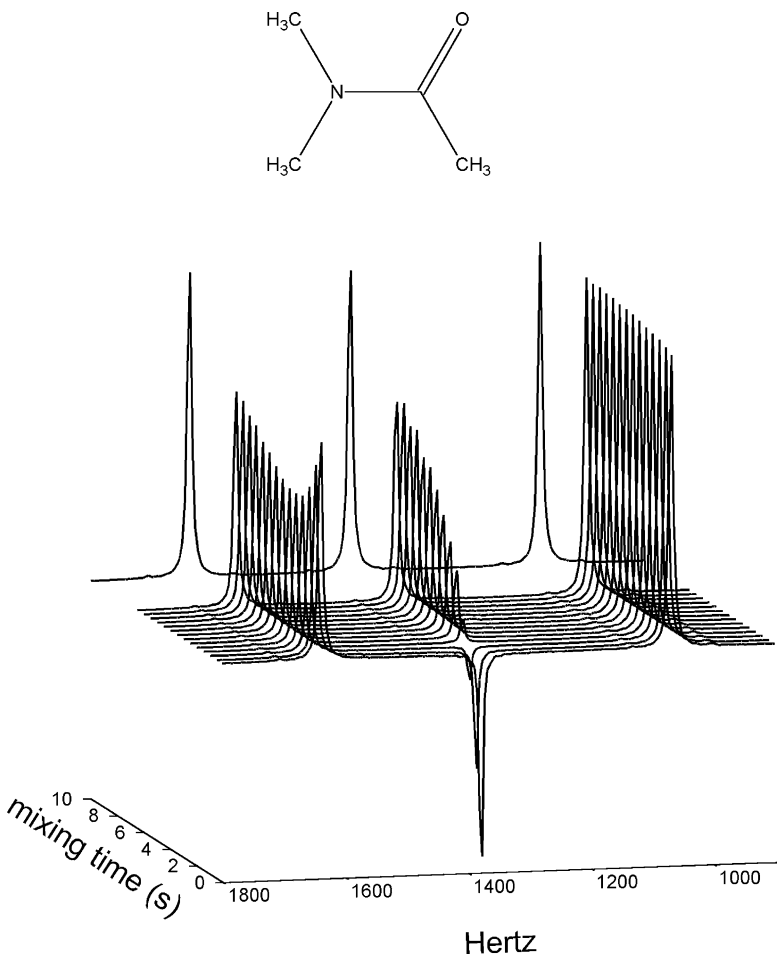

Fig. 6. Proton selective inversion experiment at 500 MHz on dimethylacetamide (structure shown in the figure) at 323 K. The low frequency signal is the acetyl methyl and the two other signals are due to the *N*-methyls, which are in slow exchange. One of the *N*-methyls was inverted at the beginning of the experiment, then the z magnetizations were allowed to relax for a series of mixing times before being measured with a $\pi/2$ pulse. The transient in the non-inverted signal is characteristic of slow exchange.

(Fig. 9). The *N*-methyls are strongly affected by the pulse spacing, but *C*-methyls are not. This is another example of the interplay between the timescale of the experiment and the timescale of the exchange.

These are all relatively simple molecules. Fig. 10 shows a ten-membered ring [30], containing two amide bonds and a disulfide, each of which usually shows restricted rotation. Amide bonds can either be *cis* or *trans*, and the equilibrium state of a disulfide is with the substituents at approximately 90° to each other, either *R* or *S*. There are many stereochemical possibilities, and in fact the molecule shows five different conformations in solution, all interconverting. Four of the barriers were determined, along with the equilibrium energies of each conformer, giving an extremely detailed experimental picture of the potential energy surface.

Finally, Fig. 11 shows a slightly more exotic case. The lowest spectrum shows the ^{13}C CP/MAS spectrum of dimethylsulfone, at room temperature, showing typical spinning sidebands. As the temperature is raised, the molecule can reorient around its

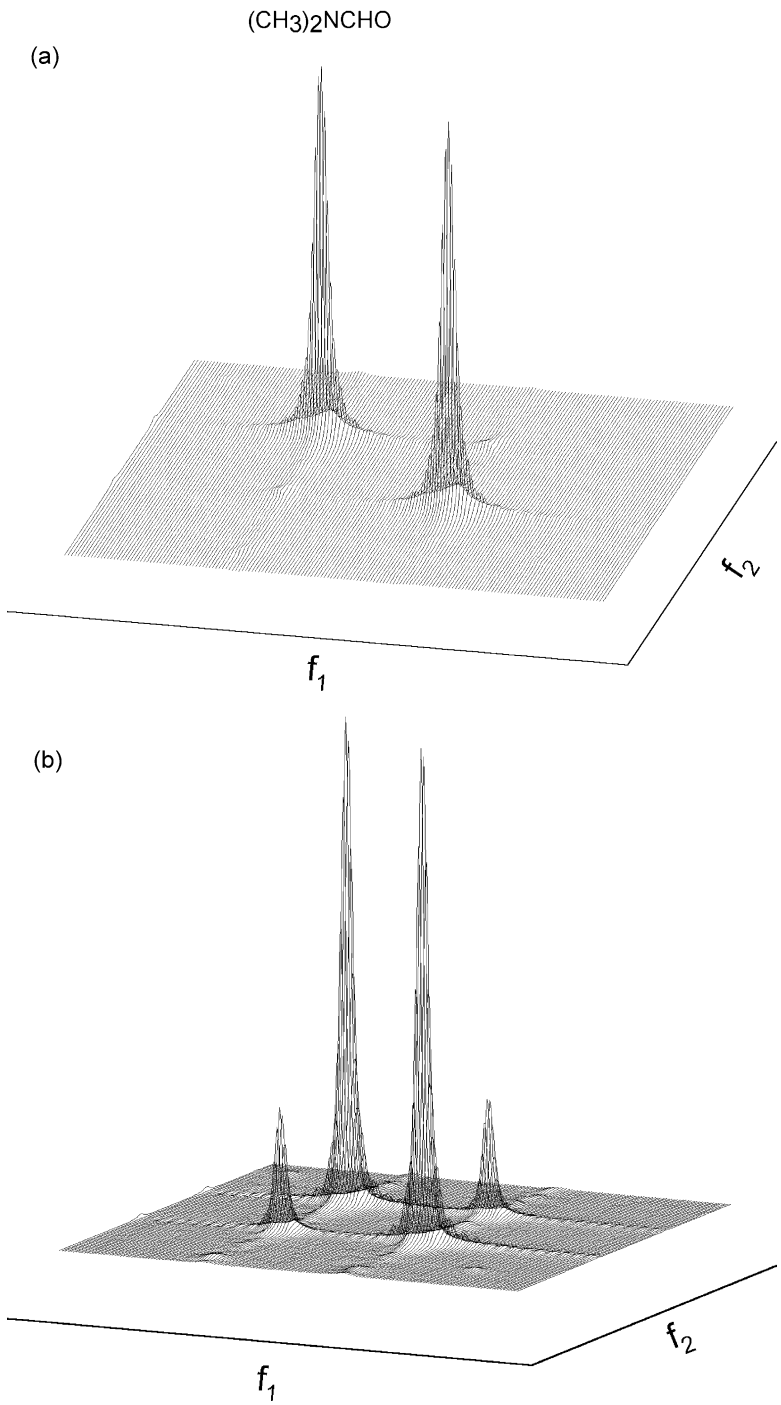

Fig. 7. Results of an EXSY experiment at 500 MHz on the two *N*-methyl signals in dimethylformamide, $(CH_3)NCHO$. Spectrum 7a is for a very short mixing time (0.01 s), so no exchange cross-peaks are visible. Spectrum 7b is for a longer mixing time (1.0 s), and shows the cross-peaks. Fig. 20 shows one-dimensional slices from these spectra, as well as for other mixing times.

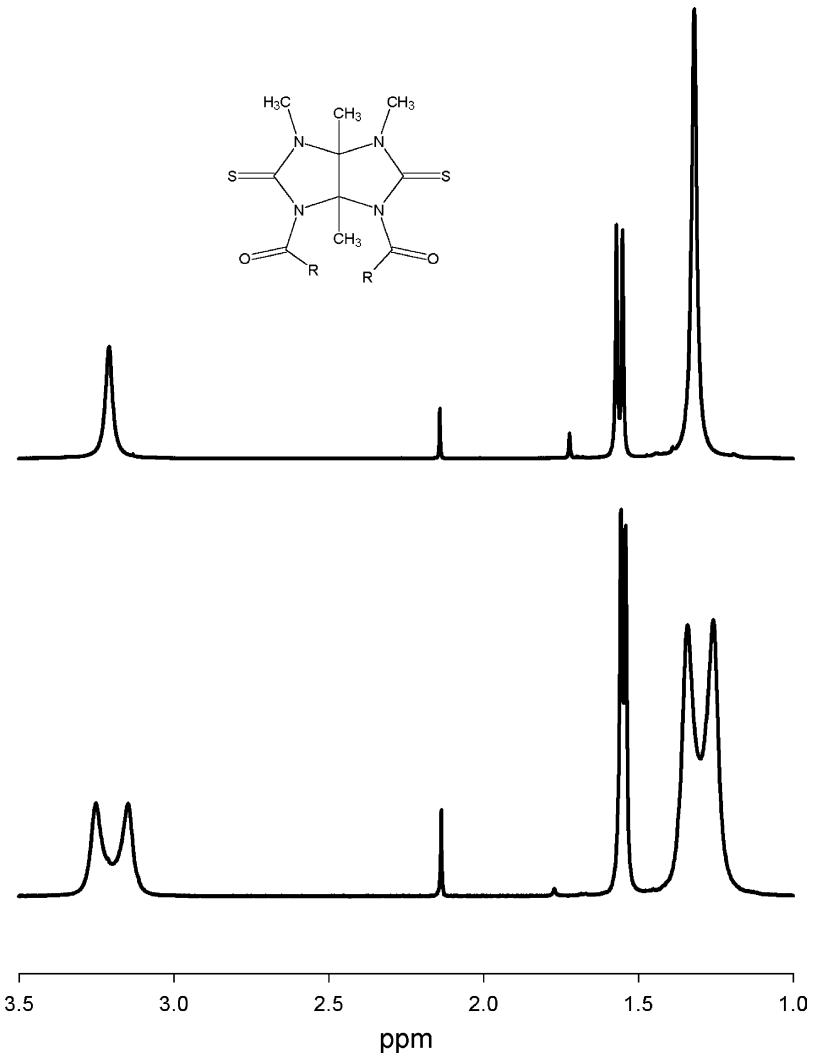

Fig. 8. Proton NMR spectra of glycoluril derivative (structure shown in the figure with the R groups being *t*-butyl) above and below the coalescence point. Because of steric and electronic effects, the twisting of the acyl groups is asymmetric, so we have atropisomers. The peaks near 1.3 ppm are the *t*-butyl protons, the peaks at 1.55 ppm are due to the methyl groups at the ring fusion, and the peaks near 3.3 ppm are the *N*-methyls. We are grateful to Dr Paul Harrison for the gift of this sample.

two-fold axis, so it makes a convenient model for exchange in the solid state [31,32]. The spinning sidebands are not magnetic sites as such, but their behaviour is reminiscent of liquid-state spectra.

These are some examples of the effects of chemical exchange. Later in the review, we will come back to some of these examples and discuss them in more detail. First, we give a more detailed introduction, a thorough discussion of the theory, some comments on exchange effects in solid-state NMR, and an analysis of fitting experimental data to theoretical lineshapes. First, we need to put chemical exchange into context.

2. History and scope

The effects of chemical exchange on NMR spectra were discovered about the same time (and in the same

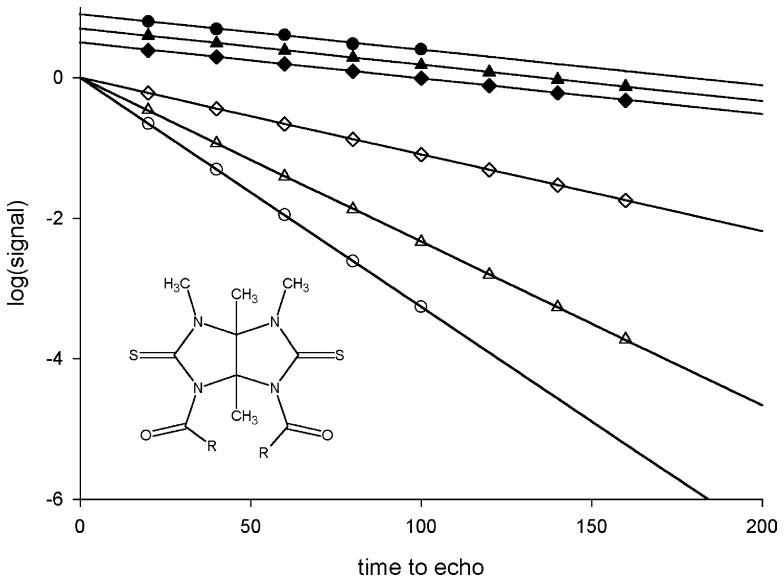

Fig. 9. Semi-logarithmic plot of peak intensity vs. time to echo in a CPMG T_2 experiment performed on the glycoluril derivative shown in Fig. 8. The three sets of data (circles, triangles, diamonds) represent π pulse spacings of 20, 5 and 2 ms, respectively. The open symbols represent the *N*-methyls, and the filled symbols, the ring fusion methyls. The signals undergoing exchange show a dependence on refocussing time, but the others do not.

laboratory) as the scalar spin–spin coupling. In fact, Gutowsky writes [33] that there was some initial confusion in the interpretation of the two peaks in the ^{19}F spectrum of PF_5. Were they the axial and equatorial fluorines (two lines in a ratio of 2:3), or was it the scalar coupling to ^{31}P in the presence of fast exchange (two equal lines)? Given the unreliable intensity measurements of the time, both were plausible explanations. When Fourier transform instruments were first available, there was some discussion [34] as to whether the FT lineshape of an exchanging system truly corresponded to the continuous-wave one. These concerns are now part of history.

The classic example of exchange phenomena involves *N*,*N*-dimethylamino groups bonded to a π system: a carbonyl in an amide, or an aromatic ring. Fig. 1 shows some experimental data. At low temperature, there is only very slow rotation about the bond joining the dimethylamino group to the ring. Interaction of the nitrogen lone pair with the π system gives some partial double-bond character and a significant barrier to rotation. In a rigid molecule, the two methyl groups are inequivalent and show two separate signals. As the temperature of the sample is raised, the rotation becomes faster, the lines in the spectrum broaden, coalesce, and finally sharpen into a single peak. The coalescence happens when the reaction rate matches an 'NMR timescale', i.e. when the rate is comparable to frequency difference between the Larmor frequencies of the two sites. Note the use of *an* NMR timescale, rather than

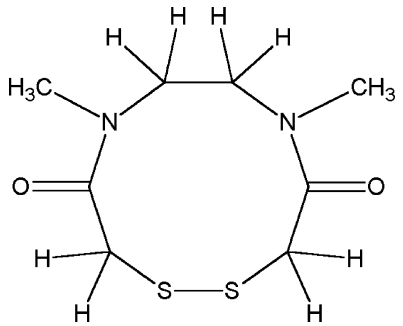

Fig. 10. *N*,*N*′-[dimethyl-(2,2′-dithiobisacetyl)]ethylenediamine, a ten-membered ring compound which shows five observable conformations in solution, all in exchange with each other [30]. The amide bonds can be *cis* or *trans* and there is restricted rotation about the disulfide bond. We thank Dr Russell Bell and Dr John Valliant for the sample.

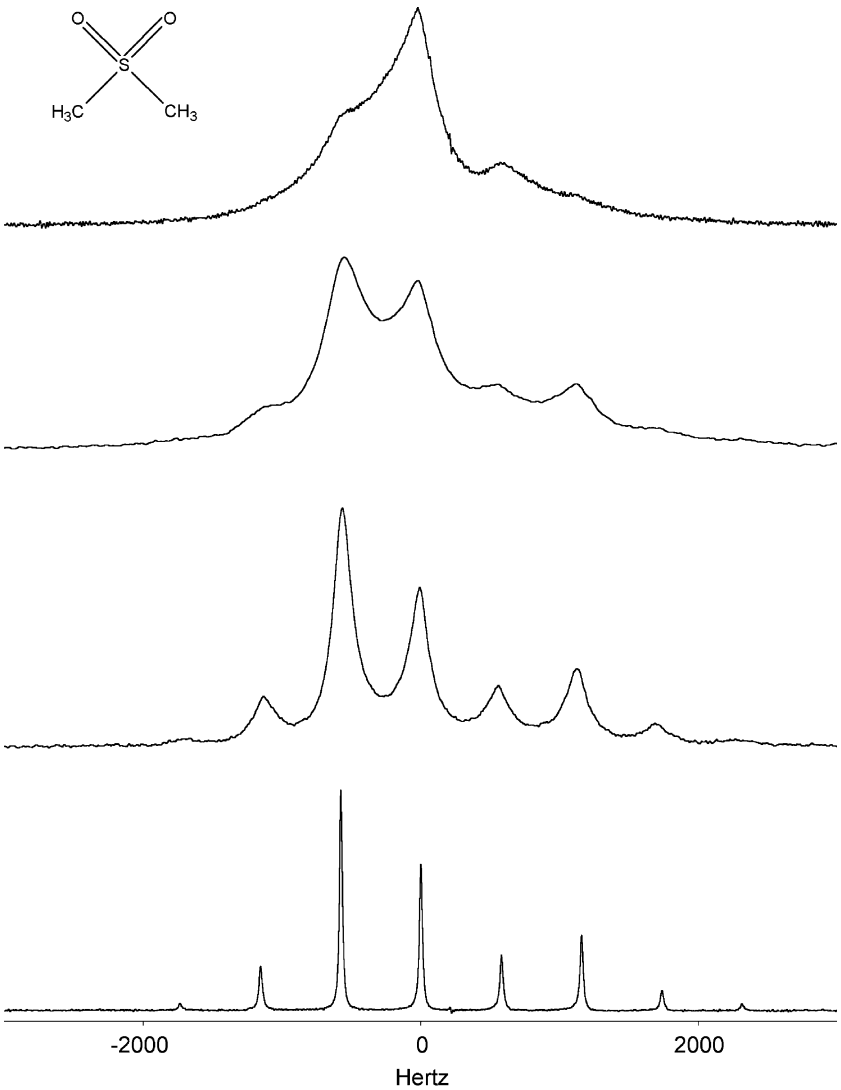

Fig. 11. CP/MAS spectra of the methyl carbons in dimethylsulfone, $(CH_3)_2SO_2$, (structure shown in the figure) as a function of temperature [32]. The rotation about the two-fold axis in the crystal causes coalescence of the spinning sidebands.

the NMR timescale. Arguments based on timescales are extremely useful, but the timescale will vary widely, depending on the system and the experiment.

There are several important parts to the study of chemical exchange in NMR. Perhaps the first is whether dynamics is observable or not. Temperature-dependent lineshapes, or cross-peaks in an EXSY spectrum strongly indicate that the molecule is not simply a fixed, rigid system. The next is the spectroscopic problem of how dynamics affect the spectrum. Once we understand the spectrum, and have measured the dynamics, what does it tell us about the molecules involved? It would be impossible to cover all the aspects and applications of chemical exchange in NMR. Therefore, the aim of this review is to develop the basic spectroscopic principles, then to illustrate the effects in a wide range of applications.

The system in Fig. 1 is a simple example, but it illustrates all the basic principles. In the absence of dynamics, the two methyl groups have different Larmor frequencies. There is some dynamic process that takes a given nucleus from one site to another. As the rate of the process approaches the frequency difference between the sites, there are dramatic changes to the spectra. For faster rates, the spectrum will converge to a fast exchange limit. The basis of describing chemical exchange is to define the sites and the processes.

A site means a magnetic environment. This is defined by all the interactions that determine the resonance frequency: chemical shielding (isotropic and anisotropic), scalar coupling, quadrupole coupling for spins with quantum numbers greater than 1/2, etc. The process is a mechanism, which carries a nucleus from one site to another. This is often a change in one of the many types of stereochemistry [35]. The process is also assumed to be instantaneous—the NMR spectrum contains no information on the course of the reaction, just the initial and final states. Liquids provide the most familiar examples. The process can be intramolecular rotation around a bond, the chair–chair interchange in cyclohexane, or the scrambling of ligands in a coordination complex. One important type of intramolecular exchange, called mutual exchange, occurs when the molecule as a whole is the same after the exchange—only the nuclei have been permuted. Alternatively, the process can be intermolecular exchange of coordinated and free ligands, exchange of a proton on an OH group with those in the water molecule, etc. Note that although the intermolecular exchange shows second-order kinetics on a macroscopic scale, the NMR spectrum is always governed by pseudo-first order kinetics. This can be rationalized by considering that NMR observes only a small fraction of the total number of spins in the sample. The individual spin we observe is exchanging with a vast excess of the other spins—see, for example, Refs. [36–39] for a further discussion. The process can change either the chemical shielding, or the scalar coupling, or both. In an oriented medium (solid or liquid crystal), the resonance frequency depends on the orientation of the molecule. Reorientation of the molecule (or part of it) will cause the magnetic environment of a nucleus to change and produce exchange effects in the NMR spectrum. Magic-angle spinning (MAS) NMR of solids introduces a further timescale into the problem: the spinning rate, as in Fig. 11. The spectra in all these cases will look quite different, but the underlying principles are the same.

One of the central ideas is that all these spectra are sums of transitions. The lowest spectrum in Fig. 1 is clearly so. For the other spectra, the decomposition of the lineshape into two transitions is less clear. However, they all can be expressed as a sum of two Lorentzian-type transitions [40], provided we allow the individual transitions to have unusual widths and phases, as in Fig. 12. This concept will lead us to a general description based on frequencies and transition probabilities that are complex, rather than the familiar real numbers.

We concentrate on the effects of exchange on the spectrum, but similar principles apply in the effect of exchange on spin–lattice relaxation times. If a spin has different relaxation times in two unresolved, but different sites, the observed relaxation will be a sum of two exponentials, in the absence of exchange [41]. If the spin is exchanging quickly between the sites, relaxation will follow a single exponential with an averaged rate. This is very similar to the exchange between resolved sites, considered in the time domain. In the FID for two resolved sites, the exchange averages two oscillatory exponentials; in

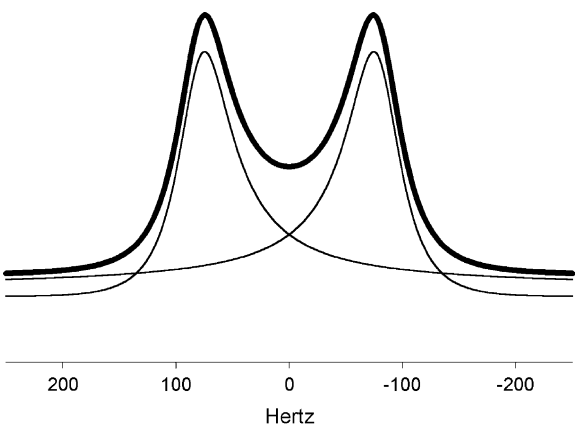

Fig. 12. Decomposition of a pre-coalescence lineshape (heavy line) into two individual transitions (Eq. (31)) (light lines), for two equally populated uncoupled sites. The transitions are distorted in phase and linewidth, which can be described by a complex-valued transition probability and frequency. See Fig. 14 for the lineshape past coalescence.

relaxation, the exchange averages two decaying exponentials. One serious complication to relaxation work is that it is much more difficult to resolve a decay into a sum of exponentials [42]. However, if the two sites cannot be resolved in the spectrum, relaxation measurements may be able to separate them. A major application of this work is the state of water in heterogeneous systems, with particular relevance in the field of NMR imaging [43–46].

Of course, relaxation is affected even if the individual sites have different resonance frequencies. In measuring a spectrum near coalescence, we assume the spin system is at equilibrium before the pulse, and that broadening due to spin–spin relaxation is relatively insignificant. If the relaxation affects the lineshape, your experimental technique may well need improvement. In slow exchange, however, selective inversion T_1 experiments [27] (Fig. 6) give excellent rate data. In fast exchange, when the spectrum has coalesced to a single line, T_2 measurements can extract rates. These results will all come from a general analysis of chemical exchange.

This review will start with the effects of chemical exchange on the lineshapes of 1D NMR spectra. This regime, where the rates are comparable to the frequencies, is called intermediate exchange. The development will describe the evolution of the density matrix in time, which is the most general case. Converting the time domain signal to a spectrum is easy. If the effects of chemical exchange during a pulse sequence are needed, the time domain is clearly the correct approach. In slow exchange and fast exchange, the spectrum itself is not sensitive to the exchange rate, so these regimes are usually studied by spin relaxation methods. The principles of these methods will also be described. Here we will also stray into the second dimension, since 2D NMR is important in mapping out slow chemical exchange. Solid-state NMR offers some new phenomena due to chemical exchange. For instance, if the exchange is comparable to the spinning rate, the TOSS sideband suppression technique starts to breakdown. Furthermore, the averaging of the interactions in the solid state (depending on the motion) does not necessarily yield an isotropic spectrum. The characteristic changes in deuterium powder patterns provide an excellent probe for dynamics. The effects of exchange on solid-state NMR will be briefly covered, but it is properly a further study. Finally, we usually want to extract a rate for the exchange, by fitting the experimental data to the calculated model. Fitting data is a large subject in itself, so we will concentrate on the NMR applications. It is our opinion that the most accurate data come from selective inversion experiments on systems in slow exchange, where accuracies of a few percent are attainable. There is far too much published work for this review to be complete, but we hope to touch on most of the recent major applications. We also hope to give a sufficiently good theoretical background to allow unfamiliar situations to be analyzed easily.

Chemical exchange is covered in almost all of the standard NMR texts, and there are several specific books [3–7] and reviews [8,9,12,47]. There are also many recent reviews [13,48–55], useful pedagogical papers [56–59], and many recent illustrations of the state of the art [60–107].

3. Kinetics and thermodynamics

Besides providing interesting spectroscopy, chemical exchange gives unique insights into molecular structure. Exchange involves the passing of the molecule through a transition state, at the top of a kinetic barrier. Measurements of the rate as a function of temperature or other parameters are one of the few ways of experimentally determining the height of the barrier. This measurement can then be compared to increasingly accurate molecular structure calculations.

The dependence of reaction rate, k, on temperature, T, was empirically described by Arrhenius [108] in Eq. (1)

$$k = A\exp(-\Delta E^{\dagger}/RT). \tag{1}$$

In this equation, A is the pre-exponential factor, R is the gas constant and $\Delta E^{\dagger}$ is the energy of activation. Later, Eyring put this relation on a firmer theoretical basis. Eyring's equation gives the rate constant as in Eq. (2)

$$k = \frac{k_B T}{h}\exp(-\Delta G^{\dagger}/RT) = \frac{k_B T}{h}\exp(\Delta S^{\dagger}/R - \Delta H^{\dagger}/RT). \tag{2}$$

In this equation, k_B is Boltzmann's constant, h is Planck's constant and $\Delta G^{\dagger}$ is the free energy of activation. Some authors [108] include a transmission coefficient as well, but this is not universal.

The rate we measure is the rate of transfer from one site, A, to the other, B. However, the system is in dynamic equilibrium, so there is a reverse rate as well, as in Eq. (3)

$$A \underset{k_r}{\overset{k_f}{\rightleftharpoons}} B. \tag{3}$$

If the two sites do not have equal populations, then the ratio of the forward and reverse rates are related to the equilibrium constant, K, by

$$K = \frac{[B]}{[A]} = \frac{k_f}{k_r}. \tag{4}$$

It is important to remember that the equilibrium constant itself is temperature-dependent, through the relation to the standard free energy difference between the two sites, ΔG^0

$$K = \exp(-\Delta G^0/RT). \tag{5}$$

In order to analyze experimental data, it is customary to plot the natural logarithm of k/T against $1/T$, an Eyring plot. The slope and the intercept of the straight line are given by Eq. (6), in which log means natural logarithm. The constant term in the intercept (if the rate is in s^{-1}), is obtained from $k_B/h = 2.0842 \times 10^{10}\ s^{-1}\ K^{-1}$, whose natural logarithm is 23.76024.

$$\text{slope} = \Delta H^{\dagger}/R$$

$$\text{intercept} = \log\left(\frac{k_B}{h}\right) + \Delta S^{\dagger}/R \tag{6}$$

Fig. 13 gives an example of this plot for the exchange of the aldehyde group in furfural between the O–O *cis* and *trans* conformations [109]. The constant term has been subtracted, so the y-axis intercept gives the entropy directly.

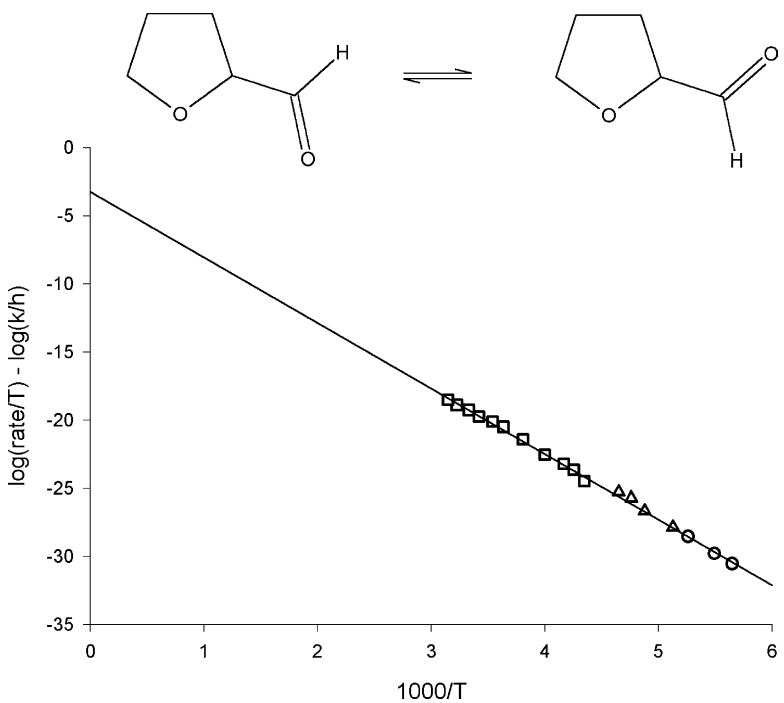

Fig. 13. Eyring plot (log(rate/T) vs. $1/T$) of the rates of *cis–trans* isomerization in furfural, (structure and process shown in the figure) [109]. Rates were determined by three complementary techniques. The squares represent data obtained by offset-saturation T_2 methods, the triangles represent lineshape measurements, and the circles represent selective inversion data.

Temperature is the most accessible experimental variable, but pressure is also a possibility. Studies of the exchange rate as a function of pressure provide a volume of activation—the effective volume change between the ground and transition states [84,110]. Although this type of experiment requires a specialized probe, it provides unique information on the transition state.

From temperature-based measurements, the problem of determining the entropy and enthalpy of activation is illustrated in Fig. 13. It is common to quote the free energy of activation, which is equivalent to quoting the rate, since all the other terms are constants. For comparison purposes, the free energy of activation is often converted to a value appropriate to 298 K, either by extrapolation or interpolation of the Eyring plot. If possible, it is good to break the free energy into its enthalpy and entropy contributions. The enthalpy is straightforward, since it is given by the slope of the Eyring plot. Care must be taken, since rate measurements from lineshapes are susceptible to biases [111]. An assumption must be made of the natural linewidth in the absence of exchange. If this assumed linewidth is too large, then the fitted rates will be underestimated in slow exchange, but overestimated in fast exchange. The slope of the Eyring plot would then give an overestimate of the enthalpy. Careful technique can minimize these problems, to provide enthalpy estimates that are reliable to a few kJ mol^{-1}. If electronic structure calculations are used to estimate the barrier, this number is often more appropriately compared to the enthalpy of activation.

The entropy is more problematic, since it is obtained from the intercept of the Eyring plot at $1/T = 0$. Even for the data in Fig. 13 [109], this involves a significant extrapolation. These furfural data represent exchange rate measurements of a temperature range of well over 100 °C, and a range of rates that vary by more than six orders of magnitude. Many kinetic measurements are over a much more restricted temperature range, so the errors inherent in extrapolating to $1/T = 0$ are much worse. Entropies of activation in the literature must be examined critically.

For intramolecular exchange, it is expected that the entropy change between the ground state and the transition state should be close to zero. If the process is a simple conformational change in a small molecule, there is little reason to expect that the transition state is significantly more or less ordered than the ground state. For biological macromolecules, entropy plays a much more significant role [112]. However, there are many small molecule cases [113–119] in which the entropy of activation is significantly non-zero. The significance of these non-zero entropies is not clear, but they are often interpreted as solvent re-organization. If the molecule is sufficiently volatile, studies of exchange in the gas phase [49,120] can give the true intramolecular barriers.

Therefore, careful rate measurements over a wide range of temperatures can give the barrier to exchange, and separate it into entropy and enthalpy effects. However, the latter are usually much better determined. In order to extract a rate from an NMR spectrum, it is essential to understand how chemical exchange affects the spectrum.

4. Theory

We will try to take a unified approach to the many different manifestations of chemical exchange in NMR. In particular, we will spend a good deal of time with the equally populated two-site exchange problem, solving it in different ways. Once we understand this simple system, more complex problems seem less daunting.

Let us start with a single spin-1/2. In the time domain, the magnetizations (or, more generally, the coherences) are governed by first-order differential equations. Let ρ represent these coherences, without specifying whether this is a single magnetization or a full density matrix. Its time dependence is given by

$$\frac{\partial}{\partial t}\rho = (\mathrm{i}\omega_0 - r)\rho. \tag{7}$$

For a single magnetization, the solution, Eq. (8), says that ρ oscillates with frequency ω_0 and decays at a rate of r

$$\rho(t) = \rho(0)\mathrm{e}^{\mathrm{i}\omega_0 t}\mathrm{e}^{-rt}. \tag{8}$$

Fourier transformation of Eq. (8) gives the spectrum in the frequency-domain, as a function of

the frequency, ω :

$$\rho(\omega) = \rho(0)\frac{1}{\mathrm{i}(\omega_0 - \omega) - r} = -\rho(0)\left(\frac{r}{(\omega_0 - \omega)^2 + r^2} + \mathrm{i}\frac{(\omega_0 - \omega)}{(\omega_0 - \omega)^2 + r^2}\right). \quad (9)$$

In the frequency-domain, Eq. (9) corresponds to a Lorentzian line, whose position is given by ω_0 and whose width is determined by r. Normally, we phase correct the spectrum so that the real part of Eq. (9) is displayed—the familiar absorption lineshape.

If there are two equally populated sites ρ_1 and ρ_2, exchanging at a rate of k, then the time dependence of the whole system is given by

$$\frac{\partial}{\partial t}\rho_1 = (\mathrm{i}\omega_1 - r_1)\rho_1 - k\rho_1 + k\rho_2$$
$$\frac{\partial}{\partial t}\rho_2 = (\mathrm{i}\omega_2 - r_2)\rho - k\rho_2 + k\rho_1. \quad (10)$$

The solution to this equation is now more complicated, but it still consists of a sum of decaying exponentials. The spectrum will always be a sum of Lorentzian lines. The phase, intensity, position and width of the lines may be sensitive functions of the exchange rate, but the form of the spectrum is very simple. The spectrum without exchange is a sum of Lorentzian lines, and so is the spectrum including exchange.

Eq. (10) is the prototype for all the systems with which we will deal, from simple two site, single-line spectra to the spinning sidebands in a MAS spectrum. The differences will be in how the equations are set up, and the details of the solution.

4.1. Bloch equations

The classic derivation of the lineshapes in Fig. 1 comes from coupled sets of Bloch equations [1,2,121]. The lineshape is treated as a single entity, and is not obviously related to non-exchanging systems. The equations also contain a B_1 observing field, in order to extract the signal. This is appropriate for systems of uncoupled spins observed with continuous-wave spectrometers; we watched as the pen traced out the shape. However, the approach is limiting—it does not treat coupled systems, the observing field is not needed, and the equations give little guidance on the time domain behaviour essential for Fourier transform spectroscopy. For a general system, a density matrix treatment is necessary [9,122].

To clarify the density matrix approach, we repeat the Bloch equations derivation, then show its analogies to a simple time-dependent density matrix calculation. This calculation is a specific example of a general approach, applicable to all exchanging systems. The end result is that the lineshape for any exchanging system is conceptually very similar to its static spectrum. The lineshape is always a sum of individual transitions, but in the exchanging system, the lines may be distorted in position, width, intensity and phase by the dynamics. We are familiar with a transition having a frequency and a transition probability. The same is true for a dynamic system, except that the frequency and the transition probability are complex numbers.

For a single spin-1/2, in the presence of a radiofrequency observation field, B_1, the Bloch equations, Eq. (11), predict the behaviour of the magnetizations. The spin has a magnetization, M_z, along the static magnetic field, B_0. Perpendicular to B_0 are two magnetizations, u and v, which precess around the static field at the Larmor frequency, $\omega_0 = \gamma B_0$, where γ is the magnetogyric ratio. Thus

$$\frac{\mathrm{d}u}{\mathrm{d}t} + \frac{u}{T_2} - (\omega_0 - \omega)v = 0,$$
$$\frac{\mathrm{d}v}{\mathrm{d}t} + \frac{v}{T_2} + (\omega_0 - \omega)u = \gamma B_1 M_z. \quad (11)$$

The notation can be simplified by defining a complex magnetization, M :

$$M = u + \mathrm{i}v. \quad (12)$$

In this notation, the Bloch equations become

$$\frac{\mathrm{d}M}{\mathrm{d}t} + \mathrm{i}(\omega_0 - \omega)M + \frac{1}{T_2}M = \mathrm{i}\gamma B_1 M_z. \quad (13)$$

Now, consider two equally populated sites, A and B, exchanging with each other. Assume (for simplicity) that their Larmor frequencies are at $\pm\delta$, so the average frequency is zero. The Bloch equations are

now

$$\frac{dM_A}{dt}+i(\delta-\omega)M_A+\frac{1}{T_2}M_A-kM_B+kM_A=i\gamma B_1M_{zA},$$
$$\frac{dM_B}{dt}+i(-\delta-\omega)M_B+\frac{1}{T_2}M_B-kM_A+kM_B=i\gamma B_iM_{zA}, \tag{14}$$

The observable NMR signal is the imaginary part of the sum of the two steady-state magnetizations, M_A and M_B, and it should be linear in B_1. It is assumed that the B_1 field is small, so that the equilibrium z magnetization is not perturbed. Since the system is equally populated, both the equilibrium z magnetizations are the same, M_z. The steady state implies that the time derivatives are zero, and a little further calculation (and neglect of T_2 terms) gives the NMR spectrum of an exchanging system as in

$$v=\gamma B_1M_z\frac{k(2\delta)^2}{(\delta-\omega)^2(\delta+\omega)^2+4k^2\omega^2}. \tag{15}$$

Early work (when spectra were traced out on paper) often looked for a coalescence point. At this rate (i.e. temperature), the top of the lineshape is flat. In mathematical terms, it is defined by the rate at which both the first and second derivative of the lineshape (with respect to frequency) vanishes at the average frequency. Some algebra shows that this is when

$$k_{\text{coalescence}}=\frac{\delta}{\sqrt{2}}. \tag{16}$$

Note that in this equation, δ is in radians per second, and the chemical shift difference between the sites is 2δ. Also, there are several different derivations (sometimes differing by factors of 2) of coalescence, so be aware of the parameter definitions and notation. If the Larmor frequencies (in Hz) of the two sites are ν_A and ν_B, then the rate at coalescence is given by

$$k_{\text{coalescence}}=\frac{2\pi(\nu_A-\nu_B)}{2\sqrt{2}}. \tag{17}$$

4.1.1. Bloch equations in the time-domain

In a Fourier transform spectrometer, the B_1 field used in this derivation is superfluous—the system is observed under free precession, after excitation by the pulse. Under these conditions, the coupled Bloch equations (Eq. (14)) can be rewritten in a matrix form

$$\frac{d}{dt}\begin{pmatrix}M_A\\M_B\end{pmatrix}=-(i\mathbf{L}+\mathbf{R}+\mathbf{K})\begin{pmatrix}M_A\\M_B\end{pmatrix}. \tag{18}$$

where the first matrix, **L**, (which will later be revealed as the Liouvillian, the commutator with the Hamiltonian) is

$$\mathbf{L}=\begin{pmatrix}\delta & 0\\0 & -\delta\end{pmatrix}. \tag{19}$$

The relaxation matrix, **R**, is given by

$$\mathbf{R}=\begin{pmatrix}\frac{1}{T_2} & 0\\0 & \frac{1}{T_2}\end{pmatrix}. \tag{20}$$

and the exchange matrix, **K**, is

$$\mathbf{K}=\begin{pmatrix}k & -k\\-k & k\end{pmatrix}. \tag{21}$$

Eq. (18) represents a set of first-order differential equations, whose formal solution is given by

$$\begin{pmatrix}M_A(t)\\M_B(t)\end{pmatrix}=\exp(-[i\mathbf{L}+\mathbf{R}+\mathbf{K}]t)\begin{pmatrix}M_A(0)\\M_B(0)\end{pmatrix}. \tag{22}$$

There are many (more or less dubious [123]) ways to calculate the exponential of a matrix, but the most appropriate in this case is to diagonalize it first, to obtain a diagonal matrix, $\mathbf{\Lambda}$:

$$\mathbf{U}^{-1}[i\mathbf{L}+\mathbf{R}+\mathbf{K}]\mathbf{U}=\mathbf{\Lambda}. \tag{23}$$

Note that the matrix in the exponential is not Hermitian (there are imaginary elements on the diagonal), so familiar eigenvalue relations [124] no longer hold. The eigenvalues are complex, the eigenvectors are complex, and the inverse of the eigenvector matrix is not simply the complex-conjugate transpose (left and right eigenvectors are different). However, we can still do the calculation by explicit inversion of **U**. Eq. (22) becomes as

follows:

$$\begin{pmatrix} M_A(t) \\ M_B(t) \end{pmatrix} = \mathbf{U}\exp(-\mathbf{\Lambda}t)\mathbf{U}^{-1}\begin{pmatrix} M_A(0) \\ M_B(0) \end{pmatrix}$$

$$= \mathbf{U}\begin{pmatrix} e^{-\lambda_1 t} & 0 \\ 0 & e^{-\lambda_2 t} \end{pmatrix}\mathbf{U}^{-1}\begin{pmatrix} M_A(0) \\ M_B(0) \end{pmatrix}. \quad (24)$$

We can get the eigenvalues simply by setting up the secular determinant and solving the usual characteristic equation:

$$\begin{vmatrix} i\delta + \frac{1}{T_2} + k - \lambda & -k \\ -k & -i\delta + \frac{1}{T_2} + k - \lambda \end{vmatrix} = 0. \quad (25)$$

The roots of this equation are given by

$$\lambda_{1,2} = \left(\frac{1}{T_2} + k\right) \pm \sqrt{k^2 - \delta^2}. \quad (26)$$

These eigenvalues are the (complex) frequencies of the lines in the spectrum: the imaginary part gives the oscillation frequency and the real part gives the rate of decay. If $k < \delta$ (slow exchange), then there are two different imaginary frequencies, which become $\pm\delta$ in the limit of small k. The width of these lines is given by $((1/T_2) + k)$. In fast exchange, when k exceeds half the shift difference, δ, the quantity in the square root in Eq. (26) becomes positive, so the roots are pure real. The imaginary part vanishes, since both transitions are at the average frequency, which we defined to be zero. Note that this critical point is when the rate is a factor of $\sqrt{2}$ faster than coalescence (Eq. (16)). This relation was derived by algebraic manipulation in 1970 by Reeves and Shaw [40]. This calculation means that the spectrum is still two lines, but they are both at the average chemical shift (zero, in this case), and have different widths. One line is negative in intensity, and broader, as in Fig. 14. As the exchange gets faster, the broad component gets broader and decreases in integrated intensity, so it contributes little to the observed lineshape. Relatively soon after coalescence, it vanishes, leaving a single narrow line in the limit of fast exchange.

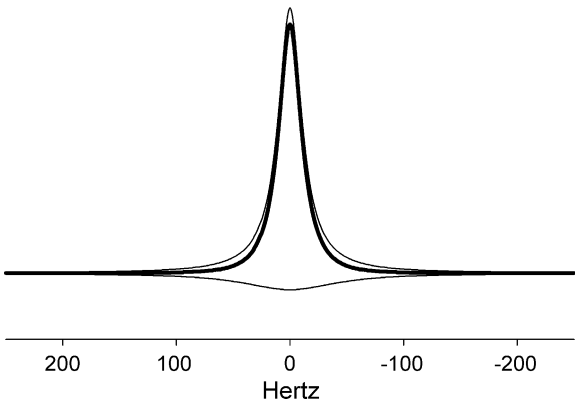

Fig. 14. Decomposition of a post-coalescence lineshape (heavy line) into two individual transitions (Eq. (31)) (light lines). Both transitions are at the average frequency, but one is broad, negative and of smaller integrated intensity. As the rate increases, this negative peak rapidly vanishes, leaving a single Lorentzian line. See Fig. 12 for the lineshape before coalescence.

The intensities of the lines, from Eq. (24), are determined by the eigenvectors of $[i\mathbf{L} + \mathbf{R} + \mathbf{K}]$. Note that the intensity may be a complex number, whose real and imaginary parts determine both the integrated intensity and the phase. The problem is simplified if we neglect the T_2 contribution. In this case, a matrix $\mathbf{U}$ of right eigenvectors can be calculated (most easily by computer programs for linear algebra), and is given by

$$\mathbf{U} = \begin{pmatrix} i(\delta + \sqrt{\delta^2 - k^2}) & i(\delta - \sqrt{\delta^2 - k^2}) \\ k & k \end{pmatrix}. \quad (27)$$

Because the original matrix was not Hermitian, the matrix of left eigenvectors (as rows) is the calculated inverse of this matrix, not simply its adjoint (its complex-conjugate transpose). However, for a 2×2 matrix, this inversion is simple. If $\mathbf{U}$ has the form (the numbers themselves may be complex):

$$\mathbf{U} = \begin{pmatrix} a & b \\ c & d \end{pmatrix}, \quad (28)$$

then its inverse is always given by

$$\mathbf{U}^{-1} = \frac{1}{\Delta}\begin{pmatrix} d & -b \\ -c & a \end{pmatrix} \quad (29)$$

$$\Delta = ad - bc.$$

If we assume that both the equilibrium z magnetizations are equal to 1, the time-domain signal, $F(t)$, from Eq. (24), is given (for any set of parameters) by

$$F(t) = \frac{(a+c)(d-b)}{\Delta} e^{-\lambda_1 t} + \frac{(b+d)(-c+a)}{\Delta} e^{-\lambda_2 t}. \tag{30}$$

Fourier transformation produces the frequency-domain spectrum, $S(\omega)$, given by

$$S(\omega) = \frac{(a+c)(d-b)}{\Delta} \frac{1}{i\omega - \lambda_1} + \frac{(b+d)(-c+a)}{\Delta} \frac{1}{i\omega - \lambda_2}, \tag{31}$$

where the parameters are defined in Eq. (26) through Eq. (29). Substituting the values from Eq. (27) into Eq. (31) gives the two-site lineshape—the real and imaginary parts give the absorption and dispersion modes. Of course, all this calculation is not necessary for a simple two-site exchange, but the approach is instructive and leads naturally to the density matrix description.

4.2. Density matrix treatment

The use of the density matrix may be intimidating, but we hope to show that it is a straightforward and natural way to describe dynamics in NMR. The definition of the density matrix, ρ, for a spin system is given in all the standard references [125–127]. The important property is that it contains all the information about the system. For any operator, $\boldsymbol{P}$, the expectation value of that observable is given by

$$\langle \boldsymbol{P} \rangle = \mathrm{trace}(\boldsymbol{P}^{\dagger} \rho). \tag{32}$$

In this equation, $\boldsymbol{P}^{\dagger}$ is the adjoint (complex-conjugate transpose) of $\boldsymbol{P}$. We need not go into the derivation or properties of the density matrix here, since it is covered in many other works. The necessary concept is that its elements encapsulate all the observables of the spin system, and the result of any particular measurement is given by Eq. (32).

For a coupled spin system, the complete density matrix description is required, except in some special cases that resemble uncoupled systems. This is because it is the nucleus that changes magnetic environments under the exchange process, not the observed spectral line. In a coupled spin system, there is no longer a one-to-one relation between nuclei and transitions. When the nucleus jumps to the other site, its relation to the transitions will change. The density matrix is needed to describe this properly.

In NMR, we often know the density matrix at the start of the experiment—we usually start at equilibrium. To calculate the density matrix at some later stage, we need its equation of motion. This is given by the Liouville–von Neumann equation

$$\frac{\partial}{\partial t} \rho(t) = -i[\boldsymbol{H}, \rho(t)] = -i\mathbf{L}\rho(t). \tag{33}$$

Note that in this equation, the first line corresponds to the usual definition of the Liouville–von Neumann equation, in which the time development of the density matrix is given by its commutator with the Hamiltonian, $\boldsymbol{H}$ (we represent operators on the spins in bold-face italics). In the second line, we have moved to Liouville space, the vector space defined by the complete set of linear operators on the spins. In this space, the density matrix becomes a vector, and the action of taking the commutator becomes a matrix in Liouville space, or a superoperator, $\mathbf{L}$ (bold-face, roman). The details of Liouville space and superoperator calculations [125,128–131] need not concern us here. The important point is that it is a natural way [122, 132] to describe dynamics in NMR.

If we include relaxation, via a Redfield-type matrix, $\mathbf{R}$, and exchange, via a Kubo–Sack or related [133–135] matrix, $\mathbf{K}$, the equation of motion of the density matrix becomes Eq. (34). Note the deliberate resemblance to Eq. (18):

$$\frac{\partial}{\partial t} \rho(t) = -[i\mathbf{L} + \mathbf{R} + \mathbf{K}]\rho(t). \tag{34}$$

Now this is a rigorous equation, valid for any spin system, coupled or uncoupled. It is solved in the same way, via the matrix exponential

$$\rho(t) = \exp(-[i\mathbf{L} + \mathbf{R} + \mathbf{K}]t)\rho(0). \tag{35}$$

Another subtlety is that we do not detect the density matrix directly, we normally detect the total magnetization along the x- or y-axis. This is represented by the operator, $\boldsymbol{I}_x$, which becomes a vector in Liouville space. Also, the definition of the scalar product in Liouville space is the trace relation, as in Eq. (32). We use parentheses [129], rather than angle brackets, to distinguish Liouville space kets, bras and inner products from the spin–space counterparts. Therefore, the measured signal, $F(t)$ is given by

$$F(t) = (\boldsymbol{I}_x|\rho(t)) = (\boldsymbol{I}_x|\exp(-[\mathrm{i}\mathbf{L} + \mathbf{R} + \mathbf{K}]t)\rho(0)). \tag{36}$$

If we have started the experiment with a simple, non-selective $\pi/2$ pulse, the density matrix at time zero is given by $\boldsymbol{I}_x$. We diagonalize the total matrix with a set of eigenvectors, $\mathbf{U}$, as before, to get

$$F(t) = (\boldsymbol{I}_x|\mathbf{U}\exp(-\boldsymbol{\Lambda}t)\mathbf{U}^{-1}\boldsymbol{I}_x)$$

$$= \sum_{i=1}^{n} (\boldsymbol{I}_x^{\dagger}\mathbf{U})_i(\mathbf{U}^{-1}\boldsymbol{I}_x)_i\exp(-\lambda_i t). \tag{37}$$

In this equation, note that the usual complex-conjugate does not appear—the inverse of $\mathbf{U}$ is $\mathbf{U}^{-1}$, not $\mathbf{U}^{\dagger}$. Eq. (37) means that the FID for the exchanging system is always the sum of decaying exponentials, since the eigenvalues, λ_i, have both imaginary and real parts. The intensity is given by the projection of the appropriate eigenvector onto $\boldsymbol{I}_x$.

This leads to a simple, physical picture of the transition probability. Each transition is represented by an eigenvector of the total Liouvillian (including relaxation and exchange). At the start of the experiment, it receives an amount of coherence from the initial $\boldsymbol{I}_x$ given by its projection. It then evolves time and contributes an amount to the detected signal proportional to its projection along $\boldsymbol{I}_x$. The intensity of the line is given by the product of how much it received at the start of the experiment and how much it contributes to the detected signal. In the absence of dynamics, this calculation simply reproduces the standard transition probability. However, the concept is applicable even in dynamic systems.

For the case of two equally populated sites, Eq. (37) becomes

$$F(t) = \begin{pmatrix} 1 & 1 \end{pmatrix} \begin{pmatrix} \mathrm{i}(\delta + d) & \mathrm{i}(\delta - d) \\ k & k \end{pmatrix} \times \begin{pmatrix} \exp(-\lambda_1 t) & 0 \\ 0 & \exp(-\lambda_2 t) \end{pmatrix} \times \begin{pmatrix} \dfrac{k}{\Delta} & \dfrac{-\mathrm{i}(\delta - d)}{\Delta} \\ \dfrac{-k}{\Delta} & \dfrac{\mathrm{i}(\delta + d)}{\Delta} \end{pmatrix} \begin{pmatrix} M \\ M \end{pmatrix}. \tag{38}$$

In this equation, the population of each site is M, the vector on the left represents $\boldsymbol{I}_x^{\dagger}$, the eigenvalues are from Eq. (26) and d and Δ are given by

$$d = \sqrt{\delta^2 - k^2}, \qquad \Delta = 2\mathrm{i}k\sqrt{\delta^2 - k^2}. \tag{39}$$

Recall that k is the rate and δ is half of the frequency separation of the two sites, in rad s^{-1}. Some algebraic manipulation will produce a lineshape identical with Eq. (15).

We have now solved the two-site equally populated lineshape problem three ways, and that is enough. We have demonstrated the equivalence of the classic derivation to a full density matrix treatment. The density matrix treatment now serves as a prototype for the solution of more complex problems.

4.3. More complex systems

If the populations are not equal, then forward and reverse rates, k_f and k_r, must be different:

$$A \underset{k_\mathrm{r}}{\overset{k_\mathrm{f}}{\rightleftharpoons}} B. \tag{40}$$

The principle of detailed balance relates the equilibrium values of the z magnetizations, thus

$$k_\mathrm{f} M_A = k_\mathrm{r} M_B. \tag{41}$$

Note that the starting density matrix must be population weighted, since the z magnetizations at the start of the experiment are determined by the Boltzmann distribution. However, once excited, each spin is detected equally, so the detector is not population weighted. In this case, Eq. (38)

becomes

$$F(t) = \begin{pmatrix} 1 & 1 \end{pmatrix} \mathbf{U} \begin{pmatrix} \exp(-\lambda_1 t) & 0 \\ 0 & \exp(-\lambda_2 t) \end{pmatrix} \times \mathbf{U}^{-1} \begin{pmatrix} M_A \\ M_B \end{pmatrix}. \quad (42)$$

The kinetic matrix in this case has the form

$$\mathbf{K} = \begin{pmatrix} k_\mathrm{f} & -k_\mathrm{r} \\ -k_\mathrm{f} & k_\mathrm{r} \end{pmatrix}. \quad (43)$$

Note that the columns must sum to zero, otherwise spins will be lost. Also, the vector of equilibrium populations must be an eigenvector of the kinetic matrix with eigenvalue zero. Otherwise, the equilibrium populations would change with time, according to the equation of motion. This is a general statement of the principle of detailed balance.

For a two-site case, the kinetic matrix is easy to set up, but larger kinetic schemes are more complex [30,136]. Consider a three-site system. There are now six rates, but not all of them are independent, thus

$$\mathbf{K} = \begin{pmatrix} k_\mathrm{f}^{AB} + k_\mathrm{f}^{AC} & -k_\mathrm{r}^{AB} & -k_\mathrm{r}^{AC} \\ -k_\mathrm{f}^{AB} & k_\mathrm{r}^{AB} + k_\mathrm{f}^{BC} & -k_\mathrm{r}^{BC} \\ -k_\mathrm{f}^{AC} & -k_\mathrm{f}^{BC} & k_\mathrm{r}^{AC} + k_\mathrm{r}^{BC} \end{pmatrix}. \quad (44)$$

Since we are dealing with a system at equilibrium, it is easy to measure the relative populations of each site. If we define an equilibrium constant for the AB reaction as

$$K^{AB} = \frac{M_B}{M_A} = \frac{k_\mathrm{f}^{AB}}{k_\mathrm{r}^{AB}}, \quad (45)$$

and the others analogously, we can rewrite Eq. (44) as

$$\mathbf{K} = \begin{pmatrix} K^{AB}k_\mathrm{r}^{AB} + K^{AC}k_\mathrm{r}^{AC} & -k_\mathrm{r}^{AB} & -k_\mathrm{r}^{AC} \\ -K^{AB}k_\mathrm{r}^{AB} & k_\mathrm{r}^{AB} + K^{BC}k_\mathrm{r}^{BC} & -k_\mathrm{r}^{BC} \\ -K^{AC}k_\mathrm{r}^{AC} & -K^{BC}k_\mathrm{r}^{BC} & k_\mathrm{r}^{AC} + k_\mathrm{r}^{BC} \end{pmatrix}. \quad (46)$$

Furthermore, the equilibrium populations must satisfy the principle of detailed balance:

$$\begin{pmatrix} K^{AB}k^{AB} + K^{AC}k_\mathrm{r}^{AC} & -k_\mathrm{r}^{AB} & -k_\mathrm{r}^{AC} \\ -K^{AB}k_\mathrm{r}^{AB} & k_\mathrm{r}^{AB} + K^{BC}k_\mathrm{r}^{BC} & -k_\mathrm{r}^{BC} \\ -K^{AC}k_\mathrm{r}^{AC} & -K^{BC}k_\mathrm{r}^{BC} & k_\mathrm{r}^{AC} + k_\mathrm{r}^{BC} \end{pmatrix} \times \begin{pmatrix} M_A \\ M_B \\ M_C \end{pmatrix} = \begin{pmatrix} 0 \\ 0 \\ 0 \end{pmatrix}. \quad (47)$$

This is a set of linear equations, but not the most convenient form for calculation. One of the equations in this set is redundant, since the bottom equation is simply the negative of the sum of the top two. The set of equations can be reduced to

$$\begin{pmatrix} K^{AB}k_\mathrm{r}^{AB} + K^{AC}k_\mathrm{r}^{AC} & -k_\mathrm{r}^{AB} \\ -K^{AB}k_\mathrm{r}^{AB} & k_\mathrm{r}^{AB} + K^{BC}k_\mathrm{r}^{BC} \end{pmatrix} \begin{pmatrix} M_A \\ M_B \end{pmatrix} = \begin{pmatrix} k_\mathrm{r}^{AC}M_C \\ k_\mathrm{r}^{BC}M_C \end{pmatrix}. \quad (48)$$

This calculation can be generalized for more complex kinetic schemes, so that equilibrium populations and kinetic matrices can be cross-checked.

4.4. Coupled spin systems

The formal approach to exchange in a coupled spin system is much the same, but there are some complications. Here, the Bloch equations approach will not work, so the density matrix is essential. One reason is that the transitions in a coupled spin system are made up from the spin wavefunctions. These wavefunctions depend on the spectral parameters—shifts, couplings, etc. When a nucleus jumps to a different site, the parameters change, and so do the wavefunctions. Therefore, coherence associated with a single transition in one site may be distributed amongst several transitions in the other. In the single-spin case, there is only one transition, so the problem does not arise. For a coupled system, we must calculate the spectrum in each site before we consider the effects of exchange.

The appropriate technique for analyzing the spectrum of each site is the use of Liouville space [128]. Even though it was introduced into NMR (as the 'direct method') for that purpose [129], it is not a very efficient way of simply calculating a spectrum. A spectrum consists of transitions, which connect wavefunctions, so it makes sense to calculate the wavefunctions. However, exchange and relaxation connect transitions, so it makes sense to use an approach that treats the transitions as the basic objects. Transitions are one manifestation of quantum mechanical operators [137], so the vector space defined by the operators as vectors is the appropriate one. This is Liouville space.

One of the requirements for a Euclidean vector space is a measure of length and direction of the vectors. This is provided by the scalar (or inner, or dot) product between two vectors—some operation on the vectors that produces a scalar. In Liouville space, the scalar product between two vectors, $\boldsymbol{P}$ and $\boldsymbol{Q}$, (operators in spin space) is defined by the trace of their product:

$$(\boldsymbol{P}|\boldsymbol{Q}) = \mathrm{trace}(\boldsymbol{P}^{\dagger}\boldsymbol{Q}). \tag{49}$$

The length of an operator has little relevance in spin space, but for Liouville space (where the operator is a vector), an orthonormal basis is essential. Such a basis is one in which each basis element has length one and the scalar product between two different basis vectors is zero. An orthonormal basis for a single spin-1/2 is given by the four operators:

$$\begin{aligned}
&\frac{1}{\sqrt{2}}\mathbf{1} = \frac{\text{Identity}}{\sqrt{2}} = \frac{1}{\sqrt{2}}\{|\alpha\rangle\langle\alpha| + |\beta\rangle\langle\beta|\} = |0)\\
&-I_{+} = -\{I_x + \boldsymbol{i}I_y\} = |\alpha\rangle\langle\beta| = |1_{+1})\\
&\sqrt{2}I_z = \frac{1}{\sqrt{2}}\{|\alpha\rangle\langle\alpha| - |\beta\rangle\langle\beta|\} = |1_0)\\
&I_{-} = \{I_x - \mathrm{i}I_y\} = |\beta\rangle\langle\alpha| = |1_{-1}).
\end{aligned} \tag{50}$$

The various minus signs and normalization constants make this into an orthonormal spherical tensor basis, having angular momentum properties. This is the angular momentum of the transition, which we have dubbed superspin [138,139]. The superspin quantum numbers define the notation on the right-hand side of Eq. (50). The pros and cons of various operator bases need not concern us here—the important point is that Eq. (50) provides an orthonormal basis for the four-dimensional Liouville space for a single spin-1/2.

For two homonuclear spins, A and B, there are four product operators (or four basis elements of the Liouville space) that span the single-quantum transitions. These are the appropriately normalized versions of the operators I_x^A, $I_x^A I_z^B$, I_x^B, $I_z^A I_x^B$. Consider an AB spin system, with Larmor frequencies ω_A, ω_B and a coupling constant of J. The single-quantum transitions are given by the eigenvalues and the eigenvectors of the Liouvillian in this basis. Some calculation [131] produces the Liouvillian

$$\mathbf{L} = \begin{pmatrix} \omega_A & J/2 & 0 & -J/2 \\ J/2 & \omega_A & -J/2 & 0 \\ 0 & -J/2 & \omega_B & J/2 \\ -J/2 & 0 & J/2 & \omega_B \end{pmatrix}. \tag{51}$$

If we define an angle, θ, (and denote its sine and cosine by s and c) by

$$\tan(2\theta) = \frac{J}{\omega_A - \omega_B}, \tag{52}$$

then the matrix of eigenvectors that diagonalizes the Liouvillian for an AB spin system is given by

$$\mathbf{U} = \begin{pmatrix} c & s & c & s \\ c & s & -c & -s \\ -s & c & s & -c \\ -s & c & -s & c \end{pmatrix}. \tag{53}$$

To calculate the spectrum, we need the vector which corresponds to the total $\boldsymbol{I}_x$ operator—this is given by

$$\boldsymbol{I}_x = \begin{pmatrix} 1 \\ 0 \\ 1 \\ 0 \end{pmatrix}. \tag{54}$$

If we substitute these expressions into Eq. (37), we get the familiar spectrum of an AB spin system. This is an unnecessarily complicated way of calculating an AB spectrum, but it does prepare for the exchange calculation.

Suppose we have two systems, AB and $A'B'$, which exchange with each other. Also, assume that

the populations will not be the same. The density matrix for the single-quantum transitions of the combined system is an eight-element vector in Liouville space, four elements for each of the two sites. Its evolution in time is governed by the Liouvillian and the exchange matrix, as above. And these are given by

$$-\mathrm{i}\mathbf{L}-\mathbf{K}=\begin{pmatrix} -\mathrm{i}\omega_A-k_\mathrm{f} & -\mathrm{i}J/2 & 0 & \mathrm{i}J/2 & k_\mathrm{r} & 0 & 0 & 0 \\ -\mathrm{i}J/2 & -\mathrm{i}\omega_A-k_\mathrm{f} & \mathrm{i}J/2 & 0 & 0 & k_\mathrm{r} & 0 & 0 \\ 0 & \mathrm{i}J/2 & -\mathrm{i}\omega_B-k_\mathrm{f} & -\mathrm{i}J/2 & 0 & 0 & k_\mathrm{r} & 0 \\ \mathrm{i}J/2 & 0 & -\mathrm{i}J/2 & -\mathrm{i}\omega_B-k_\mathrm{f} & 0 & 0 & 0 & k_\mathrm{r} \\ k_\mathrm{f} & 0 & 0 & 0 & -\mathrm{i}\omega_{A'}-k_\mathrm{r} & -\mathrm{i}J'/2 & 0 & \mathrm{i}J'/2 \\ 0 & k_\mathrm{f} & 0 & 0 & -\mathrm{i}J'/2 & -\mathrm{i}\omega_{A'}-k_\mathrm{r} & \mathrm{i}J'/2 & 0 \\ 0 & 0 & k_\mathrm{f} & 0 & 0 & \mathrm{i}J'/2 & -\mathrm{i}\omega_{B'}-k_\mathrm{r} & -\mathrm{i}J'/2 \\ 0 & 0 & 0 & k_\mathrm{f} & \mathrm{i}J'/2 & 0 & -\mathrm{i}J'/2 & -\mathrm{i}\omega_{B'}-k_\mathrm{r} \end{pmatrix}. \tag{55}$$

This is the general equation for the superoperators which control the evolution for two distinct AB systems in exchange. However, there is the important special case of mutual exchange of the two nuclei. In this case, the two nuclei are just permuted and the forward and reverse rates must be equal, so the following relations apply

$$\omega_{B'}=\omega_A, \qquad \omega_{A'}=\omega_B, \qquad J'=J, \qquad k_\mathrm{f}=k_\mathrm{r}=k \tag{56}$$

We can use this permutation symmetry to make the exchange work 'within' the system. We make symmetry-adapted basis functions such that the spins with the same Larmor frequency are combined, as in the matrix $\mathbf{U}$:

$$\mathbf{U}=\frac{1}{\sqrt{2}}\begin{pmatrix} 1 & 0 & 0 & 0 & 1 & 0 & 0 & 0 \\ 0 & 1 & 0 & 0 & 0 & 1 & 0 & 0 \\ 0 & 0 & 1 & 0 & 0 & 0 & 1 & 0 \\ 0 & 0 & 0 & 1 & 0 & 0 & 0 & 1 \\ 0 & 0 & 1 & 0 & 0 & 0 & -1 & 0 \\ 0 & 0 & 0 & 1 & 0 & 0 & 0 & -1 \\ 1 & 0 & 0 & 0 & -1 & 0 & 0 & 0 \\ 0 & 1 & 0 & 0 & 0 & -1 & 0 & 0 \end{pmatrix}. \tag{57}$$

We then pre- and post-multiply the matrix in Eq. (55) to get

$$\mathbf{U}^{-1}(-\mathrm{i}\mathbf{L}-\mathbf{K})\mathbf{U}=\begin{pmatrix} \mathbf{L}' & \mathbf{0} \\ \mathbf{0} & \mathbf{L}' \end{pmatrix}, \tag{58}$$

where

$$\mathbf{L}'=\begin{pmatrix} -\mathrm{i}\omega_A-k & -\mathrm{i}J/2 & k & \mathrm{i}J/2 \\ -\mathrm{i}J/2 & -\mathrm{i}\omega_A-k & \mathrm{i}J/2 & k \\ k & \mathrm{i}J/2 & -\mathrm{i}\omega_B-k & -\mathrm{i}J/2 \\ \mathrm{i}J/2 & k & -\mathrm{i}J/2 & -\mathrm{i}\omega_B-k \end{pmatrix}.$$

This means we still have a 4x4 matrix to describe an AB spin system, as in the static case (Eq. (51)). However, now the dynamics are included. This case of mutual exchange in an AB spin system is a classic problem with an analytical solution, described by Alexander [140].

The case of exchange in an AB spin system, whether mutual or not, serves as a prototype for any exchange in liquids. For any spin system, the spectral analysis of each site must be done, to set up the Liouvillian. Then the exchange mechanism must be described, to indicate which spin exchanges with which. Once these two matrices in Liouville space are set up, the combined matrix can be diagonalized using standard methods, to yield eigenvalues and eigenvectors. The observed FID or spectral lineshape can be calculated using Eq. (37). Fig. 15 shows how the exchange spectra in nitrosoaniline (from Fig. 2) can be decomposed into individual transitions. For n spins-1/2, the number of possible transitions is given

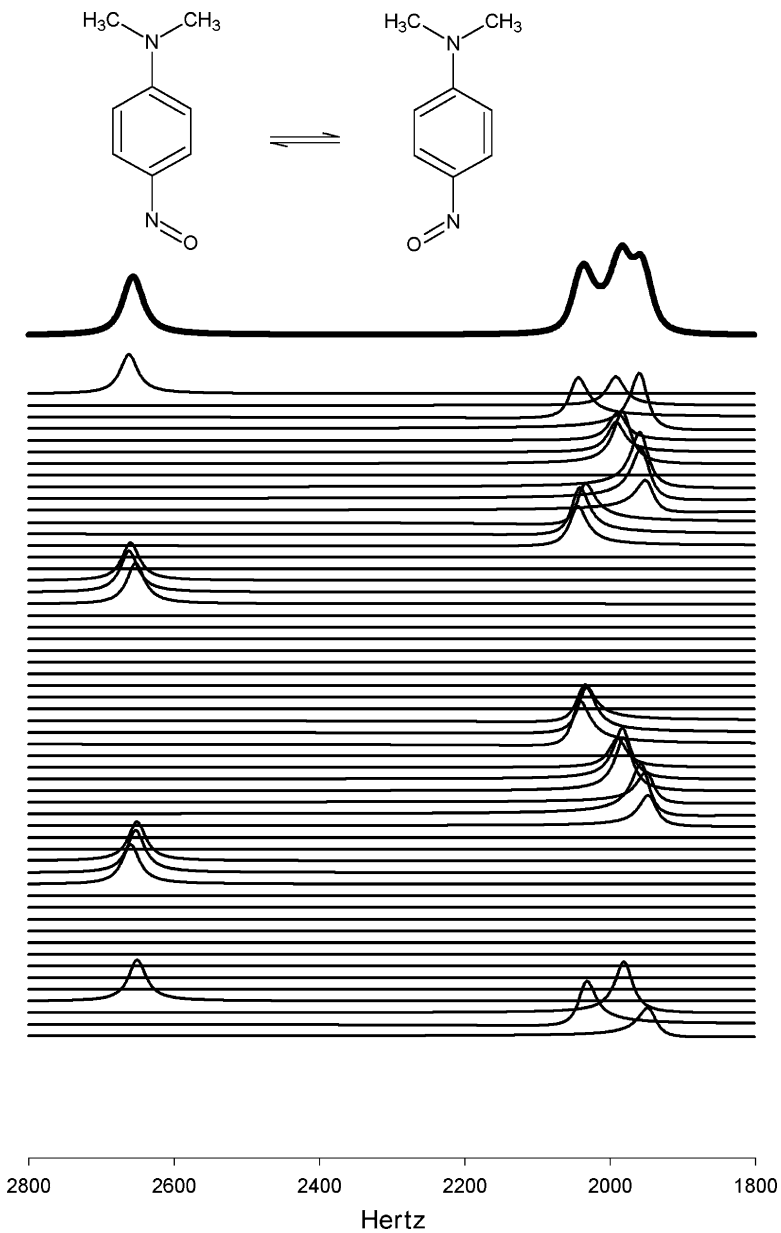

Fig. 15. Decomposition of the spectrum (top trace, heavy line) of the aromatic protons in *p*-nitrosodimethylaniline (structure shown in the figure) (spectrum from Fig. 2) into individual transitions (light lines). The exchange lineshape for a coupled spin system may be analyzed as a sum of transitions, in the same way as the two-site uncoupled case in Fig. 12. Four coupled spins-1/2 will generate 56 total transitions that make up the spectrum. Many transitions have vanishing intensity, but are plotted for completeness.

by the binomial coefficient

$$\binom{2n}{n-1},$$

which is 56 for four spins. However, as in the analysis of static spectra, many transitions have very low intensity. As with two uncoupled sites, the transitions are distorted in linewidth and phase, but each is a single line. Setting up the matrices may be tedious for

large spin systems and complex exchange mechanisms, but the formalism is always the same.

5. Slow exchange

Slow means that the exchange rate is much smaller than the frequency difference between the sites. In this case, the appearance of the spectrum is only slightly broadened by the exchange. Estimating the rate from the line broadening is hazardous, since these effects are difficult to distinguish from magnetic field inhomogeneities and other line-broadening mechanisms. It is very dangerous to assume that the linewidth can be estimated from the assumption that T_1 and T_2 are roughly equal. For instance, in the classic case of dimethylacetamide (structure in Fig. 6), there is a five-bond coupling between the acetate methyl and the *N*-methyl which is *trans* to it, giving a broadening to that line. When the question of the 'natural linewidth' becomes important, it is usually better to measure the rate from the effect of exchange on the spin–lattice relaxation.

The basic principle is quite straightforward. If the z magnetization of a site is inverted, it will relax back to equilibrium via the usual spin–lattice relaxation mechanisms. If there are two sites, an individual spin may exchange sites during the relaxation and carry its polarization. If one site is inverted selectively, then its spins may relax either by the normal spin–lattice relaxation, or by exchange with the non-inverted site. If the polarization of the two exchanging sites is different, the exchange will tend to average them. This leads to a faster return to equilibrium for the inverted site, and a transient dip in the other site, as in Figs. 6 and 16. The lower half of Fig. 16 shows the normalized intensities of both the *N*-methyl signals in dimethylacetamide following a non-selective π pulse. This is a standard inversion-recovery T_1 experiment. Both the methyl groups have roughly the same T_1, so their signals are superimposed as they both relax back to equilibrium. Their polarizations are the same, so exchange has essentially no effect on this experiment. If the T_1 values were different, the exchange will average them to some extent, so the decay rate in the lower panel is not strictly T_1. The upper panel of Fig. 16 shows the intensities of the methyls following a *selective* inversion of one of the signals, in an experiment similar to that in Fig. 6. The inverted site (triangles) relaxes much more quickly at first, then at approximately the same rate as in the bottom panel. The signal that was not inverted (circles) decreases in intensity at first, and then relaxes to equilibrium. This transient behaviour of the non-inverted site is characteristic of exchange. Both the curves in the upper panel of Fig. 16 are bi-exponential; one rate dominated by the exchange, the other by T_1. The two rates can be seen in Fig. 16, but are made obvious in the semi-logarithmic plot of the data from the selectively inverted signal in Fig. 17.

The mathematical description of this still fits the general form, Eq. (10). In particular, the z magnetizations do not oscillate, so it is only the decay terms that are important. In Eq. (34), the z magnetizations are eigenvectors of the Liouvillian, $\mathbf{L}$, with eigenvalue zero. Eq. (34) becomes

$$\frac{\partial}{\partial t}\rho(t) = -[\mathbf{R} + \mathbf{K}]\rho(t), \tag{59}$$

in which $\rho(t)$ represents only the z magnetizations. $\mathbf{R}$ is the Redfield matrix which defines all the spin–lattice relaxation rates, and $\mathbf{K}$ is the exchange matrix.

Note that this equation contains no imaginary terms, so there are no oscillations, just decays. Strictly speaking, we must include the equilibrium magnetization. As before, the formal solution is given by the matrix exponential:

$$(\rho(t) - \rho_{eq}) = \exp(-[\mathbf{R} + \mathbf{K}]t)(\rho(0) - \rho_{eq}). \tag{60}$$

In practice, the solution is calculated by the diagonalizing the matrix, as in Eq. (37).

For a system without scalar coupling, the z magnetizations can be measured by a non-selective $\pi/2$ pulse. The distinction between what we observe and the density matrix is not important in this case. We do not observe the z magnetizations directly, but the line intensities after the observe pulse reflect them faithfully. If there are n sites, we list their z magnetizations in the vector $\rho(t)$. Recall that going to Liouville space involves writing the density matrix elements out as a vector. The z magnetizations correspond to part of that large vector, and their time-dependence is not coupled to the rest of the elements of the density matrix. If at time zero, we perturb the z magnetizations from their equilibrium values, ρ_{eq}, then their return to equilibrium is

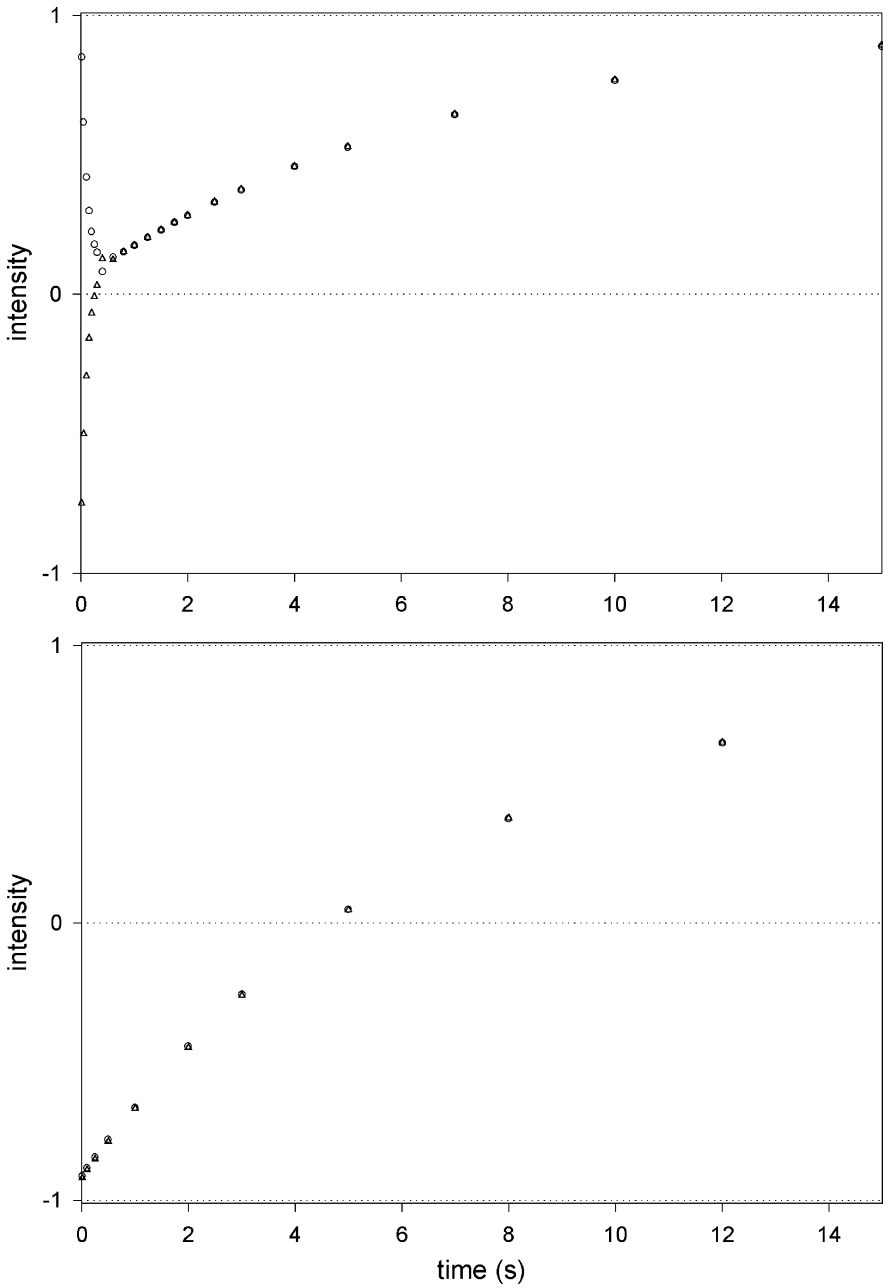

Fig. 16. Plots of line intensity vs. time for a selective inversion (top graph) and a non-selective inversion (bottom) on the *N*-methyl groups of dimethylacetamide (structure shown in the figure). Both experiments were run under identical conditions. The selective inversion data are from an experiment similar to that shown in Fig. 6, in which one signal (triangles) was selectively inverted and the other unperturbed (circles) at the start of the experiment. The system was allowed to relax for a series of times, and then the signals were measured. The non-selective inversion experiment is a standard inversion-recovery T_1 experiment. The T_1 values of the two methyl groups are similar, so the data points overlap. Chemical exchange causes rapid equilibration of the two signals in the selective inversion experiment.

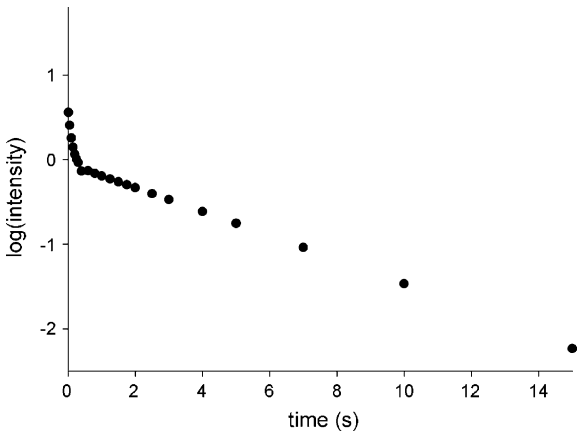

Fig. 17. Semi-logarithmic plot of the data from the selectively inverted peak (triangles) in the top graph of Fig. 16, showing the bi-exponential character. The fast rate is dominated by exchange, the slower rate is due to spin relaxation.

defined by

$$(\rho(t)-\rho_{eq}) = \mathbf{U}\exp(-\mathbf{\Lambda}t)\mathbf{U}^{-1}(\rho(0)-\rho_{eq}) = \sum_{i=1}^{n}\mathbf{U}(\mathbf{U}^{-1}(\rho(0)-\rho_{eq}))_i\exp(-\lambda_i t). \quad (61)$$

The summation shows that the decay will be a sum of exponentials, the number of terms equaling the number of sites—we have seen the case of $n=2$ in Fig. 16. However, the coefficients depend on the state of the system at time zero, $(\rho(0)-\rho_{eq})$. Because the selective inversion and the non-selective inversion represent different state of the system at time zero, the return to equilibrium is quite different, as shown in the two panels in Fig. 16. The time constants are the same, regardless of the state at time zero. The different preparations of the spin system merely highlight or suppress different terms in Eq. (61). The important point is that the preparation is somewhat under our control, so we can choose a preparation that highlights exchange: selective inversion; or hides it: non-selective inversion.

The reader will have noticed that for unequally populated sites, the matrix $[\mathbf{R}+\mathbf{K}]$ is not symmetric, so there is the possibility of non-real eigenvalues. However, provided the principle of detailed balance is obeyed, the matrix can be made symmetric by pre- and post-multiplication with a diagonal matrix that has the square root of the level populations down the main diagonal. This symmetrization may be necessary to accommodate some numerical diagonalization routines, but is not an essential step. The important point is that the eigenvalues are always real.

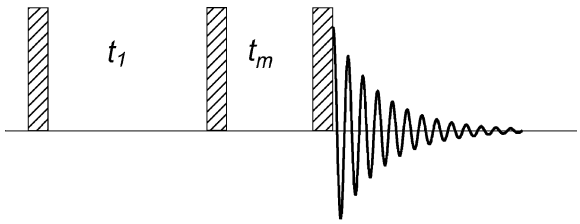

Fig. 18. Pulse sequence for EXSY. The pulses are all $\pi/2$, t_m is the mixing time, and t_1 is the regularly incremented delay that defines the second dimension.

The 2D EXSY experiment [28] is one of the most popular ways of observing slow chemical exchange. The pulse sequence, shown in Fig. 18, is the same as that of the NOESY experiment, which reveals dipolar relaxation between spins. This is hardly surprising, given the similarities between exchange and relaxation. The basis of the experiment is to look at the early stages of the exchange (or relaxation). For short values of the time t, Eq. (60) becomes

$$\rho(t) \approx (\mathbf{1} - [\mathbf{R}+\mathbf{K}]t)\rho(0), \quad (62)$$

in which $\mathbf{1}$ represents the unit matrix.

Recall that $\rho(t)$ in this case is just the vector of the z magnetizations associated with each site. Slow exchange amongst the sites (or dipolar relaxation) is represented by off-diagonal elements in the relaxation-plus-exchange matrix. In physical terms, this means that the measured relaxation rate of one site depends on the initial state of the other site. If there is no exchange or dipolar contribution, the matrix in Eq. (62) is diagonal, and the spins relax independently.

The advent of 2D NMR made all this much more convenient. In the EXSY pulse sequence (Fig. 18), we can regard the second and the third pulses as a type of saturation-recovery T_1 experiment. The signal following the observe pulse indicates how much the system has relaxed during the mixing time, t_m. The purpose of the evolution time, t_1, is to frequency-label the initial conditions of the relaxation experiment. If the initial conditions are frequency-labeled, then so are the signals following the observe pulse. A 2D Fourier transform then reveals all the sites whose initial

preparation affect the relaxation of the site being observed. This means that cross-peaks appear in the 2D spectrum. The choice of the mixing time is critical [141,142]. If it is too short, no cross-peaks will be observed; if it is too long, then the linear assumption implicit in Eq. (62) will be violated. If there are only two sites, then the volume of the cross-peak will come to a maximum and then fade. If there are multiple sites, breakdown of the linear approximation can lead to observed cross-peaks between sites that are not directly connected by exchange. During a long mixing time, a spin may exchange twice, producing a spurious cross-peak.

For two equally populated sites, the cross-peak intensities are easy to calculate. The relaxation and kinetic matrices are given by

$$\mathbf{R} = \begin{pmatrix} \frac{1}{T_1} & 0 \\ 0 & \frac{1}{T_1} \end{pmatrix} \tag{63}$$

$$\mathbf{K} = \begin{pmatrix} k_\mathrm{f} & -k_\mathrm{r} \\ -k_\mathrm{f} & k_\mathrm{r} \end{pmatrix}.$$

The eigenvalues of the combined relaxation and kinetic matrices (to be used in Eq. (61)) are given by

$$\lambda_1 = \frac{1}{T_1} \tag{64}$$

$$\lambda_2 = \frac{1}{T_1} + 2k,$$

and the matrix of eigenvectors is given by

$$\mathbf{U} = \begin{pmatrix} \frac{1}{\sqrt{2}} & \frac{1}{\sqrt{2}} \\ \frac{1}{\sqrt{2}} & -\frac{1}{\sqrt{2}} \end{pmatrix}. \tag{65}$$

Let the magnetizations after the t_1 period associated with the two sites be denoted by $M_A(t_1)$ and $M_B(t_1)$. The evolution during t_1 has frequency-labelled them, so they are distinguishable at the start of the mixing time. Eq. (61) predicts that the magnetizations at the end of the mixing time, t_m, will be given by

$$\begin{aligned} &\begin{pmatrix} M_A(t_1+t_\mathrm{m}) \\ M_B(t_1+t_\mathrm{m}) \end{pmatrix} \\ &= \begin{pmatrix} \frac{\mathrm{e}^{-t_\mathrm{m}/T_1} + e^{-t_\mathrm{m}(1/T_1+2k)}}{2} & \frac{\mathrm{e}^{-t_\mathrm{m}/T_1} - \mathrm{e}^{-t_\mathrm{m}(1/T_1+2k)}}{2} \\ \frac{\mathrm{e}^{-t_\mathrm{m}/T_1} - \mathrm{e}^{-t_\mathrm{m}(1/T_1+2k)}}{2} & \frac{\mathrm{e}^{-t_\mathrm{m}/T_1} + \mathrm{e}^{-t_\mathrm{m}(1/T_1+2k)}}{2} \end{pmatrix} \\ &\quad \times \begin{pmatrix} M_A(t_1) \\ M_B(t_1) \end{pmatrix} \\ &= \begin{pmatrix} \mathrm{e}^{-t_\mathrm{m}/T_1}\frac{1+\mathrm{e}^{-2t_\mathrm{m}k}}{2} & \mathrm{e}^{-t_\mathrm{m}/T_1}\frac{1-\mathrm{e}^{-2t_\mathrm{m}k}}{2} \\ e^{-t_\mathrm{m}/T_1}\frac{1-\mathrm{e}^{-2t_\mathrm{m}k}}{2} & \mathrm{e}^{-t_\mathrm{m}/T_1}\frac{1+\mathrm{e}^{-2t_\mathrm{m}k}}{2} \end{pmatrix} \\ &\quad \times \begin{pmatrix} M_A(t_1) \\ M_B(t_1) \end{pmatrix}. \end{aligned} \tag{66}$$

This equation says that the intensities of the diagonal peaks in an EXSY spectrum for two equally populated sites are given by the diagonal elements of the matrix, and the cross-peaks are given by the off-diagonal elements. The two functions are plotted in Fig. 19, and some experimental data (from the series of experiments in Fig. 7) are given in Fig. 20.

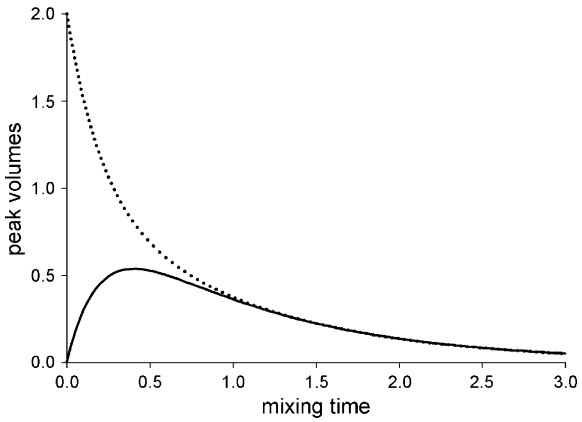

Fig. 19. Plot of the theoretical diagonal peak volume (solid line) and cross-peak volume (dotted line) as a function of mixing time in an EXSY experiment on a two-site equally populated exchange, from Eq. (66). See Fig. 20 for experimental data.

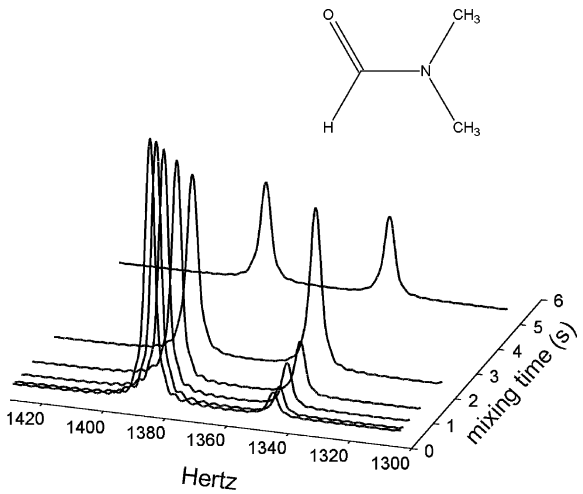

Fig. 20. Slices from a series of EXSY experiments (see Fig. 7) on dimethylformamide, as a function of mixing time, showing the diagonal peak (high frequency) and the cross-peak (low frequency).

EXSY represents an excellent way of establishing that there is slow exchange between sites. However, despite its wide popularity, it is our opinion that it is not the best way of obtaining an actual value for the rate. An estimate of the rate can be obtained from the ratio of the cross-peak to diagonal peak volumes. This is equal to the ratio of the off-diagonal term to the diagonal matrix element in Eq. (66). If this ratio is called r, then the rate is given by

$$e^{-t_m/2k} = \frac{1-r}{1+r} \tag{67}$$

$$k = \frac{t_m}{2\log\left(\frac{1+r}{1-r}\right)}.$$

Note that log means natural logarithm.

It is often recommended to repeat the EXSY experiment for a series of mixing times, and measure the cross-peak volumes [143,144] as a function of the mixing time. The slope of this line gives the rate. For multi-site kinetic schemes, the mixing times must be short, since longer times may lead to spurious cross-peaks.

However, a selective inversion experiment [142, 145–150] can be performed in approximately the same time as a single EXSY. There is no restriction to short mixing times—in fact it is important to follow the complete course of the relaxation. The data present the reaction rate in competition with the relaxation, so the rate is measured directly. There is no complication with the natural linewidth, such as occurs in lineshape methods. With suitable precautions, the selective inversion experiment can give quite accurate measurements [150]. Although all the parameters are implicit in a one selective inversion experiment, we usually find it best to do two experiments, as in Fig. 16. A normal non-selective inversion-recovery experiment is done to estimate the spin–lattice relaxation rate (even though the exchange will average the T_1 values), followed by a selective inversion experiment. The selective inversion data are more sensitive to the exchange, so we fix the relaxation rates and fit the exchange rate.

For a coupled spin system, the situation is much more complicated. If a coupled spin system is not in an equilibrium-like state, the observed spectrum will depend on the flip angle used to observe it [151–154]. Selective inversions may create such states, so the relationship between the line intensities in the spectrum and the z magnetizations is much more complex. The analysis of relaxation after selective inversions in coupled spin systems has only recently been analyzed [148,155]. However, these complications are important only if selective pulses affect different members of a multiplet in different ways. If the couplings are small enough, or the bandwidth of the pulse is such that a whole multiplet is inverted in concert, then a simple analysis is possible. The intensity of the whole multiplet can be treated like an uncoupled site, to a good approximation.

Slow exchange gives the best data, in our opinion. The exchange is balanced against spin–lattice relaxation, and very few assumptions are needed. The 2D EXSY experiment is unparalleled in revealing the presence of slow chemical exchange. However, for quantitative work, we prefer the 1D selective inversion experiments.

6. Fast exchange

This is usually defined as the regime which is well past coalescence, where the observable spectrum is essentially a single Lorentzian line as in the top spectrum in Fig. 9. The line is still broadened by

the exchange, but the broadening is comparable to the natural linewidth and broadening due to magnetic field inhomogeneity. This means that simple lineshape methods are unreliable, since the same shape can correspond to a multitude of values of rates and natural linewidths. Therefore, the contribution of exchange must be determined by a T_2 experiment, which suppresses inhomogeneous broadening and reliably measures the spin–spin relaxation time.

Both the classic CPMG and the rotating-frame $T_{1\rho}$ have been widely used. The offset-saturation method [156,157] has also been used successfully [109]. Measurements of the spin–spin relaxation time must be done carefully [158], unlike T_1 determinations with the inversion-recovery T_1 experiment,. The T_1 experiment is very robust, but the T_2 experiment can be quite sensitive to incorrect parameters in the setup.

The extent of the broadening can be calculated from the general solution given in Eq. (37). For a two-site equally populated case, there are two lines in the spectrum, both at the average Larmor frequency. Their linewidths are given by the roots of the characteristic equation, from Eq. (26). In this equation, the two sites have Larmor frequencies (in rad s^{-1}) of $\pm\delta$ (note the difference in frequency is 2δ) and an exchange rate of k, which is much larger than the frequency difference. The positions of the two lines are both at zero frequency, and the T_2 values (assuming $k \gg \delta$) are given by

$$\begin{aligned}\lambda_{1,2} &= \left(\frac{1}{T_2}+k\right) \pm \sqrt{k^2-\delta^2} \\ &\approx \left(\frac{1}{T_2}+k\right) \pm k\left(1-\frac{\delta^2}{2k^2}\right) \\ &= \left(\frac{1}{T_2}+2k\right) \text{ or } \left(\frac{1}{T_2}+\frac{\delta^2}{2k}\right). \end{aligned} \tag{68}$$

Recall that δ in this equation, as before, is half the difference in frequency between the sites, in rad s^{-1}. The frequencies at the two sites are $\pm\delta$. Since $k \gg \delta$, the line corresponding to the first eigenvalue is very broad, and moreover has a small integrated intensity—we detect only the transition associated with the second eigenvalue. In the literature, the notation and parameter definitions for this case vary considerably. In our definition, the spectrum essentially consists of a single line with an exchange contribution to its linewidth given by $\delta^2/2k$.

The problem is that we can extract from the linewidth only the ratio of the rate to the frequency separation of the two sites. If we can freeze out the exchange, i.e. slow the process (with temperature) or increase the separation (higher field), we can estimate the separation and calculate a rate. For many samples, these remedies are not available. However, provided the rate is not too fast, we can still extract a rate.

There is an inherent timescale in the experiments for measuring T_2. For the CPMG experiment, it is the timing of the refocussing π pulses, and for the $T_{1\rho}$ experiment, it is the rate of precession around the spin-locking field. If we measure T_2 at timescales that are slower than the exchange, and faster than the exchange, we will get different apparent T_2 values [159–165]. A slow timescale will give values corresponding to the observed linewidth, including exchange. A fast timescale will give values reflecting the T_2 values of the individual sites, with little influence of exchange. The dispersion in T_2 gives us an absolute estimate of the rate without the necessity for knowing the frequency separation. The general expression [163] is complicated, but the two-site equally populated case [160] is fairly simple, and is given by

$$\frac{1}{T_2} = \frac{1}{T_2^0} + k - \frac{1}{t_{CP}}\sinh^{-1}F. \tag{69}$$

where

$$F = \frac{k}{\sigma}\sinh(t_{CP}\sigma/2) \tag{70}$$

$$\sigma = [k^2-\delta^2]^{1/2}.$$

Note that our definitions differ from those in Ref. [160], but are consistent with the other equations here.

Fig. 9 showed some experimental data on a simple system, which we can freeze out, so we can get a good measure of the rate. Fig. 21 shows the fit of the data to Eq. (69). In this case, the fastest pulsing corresponded to 2 ms between the refocussing pulses, and a rate of approximately 1000 s^{-1}. The method has been applied to a variety of experimental systems [166, 167], but its range is limited. This is because the timescale of the CPMG or the $T_{1\rho}$ experiment is limited to approximately 10^4 s^{-1}—pulsing with

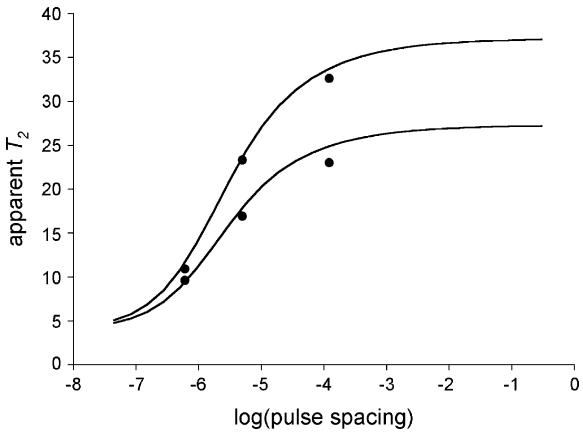

Fig. 21. Plot of apparent T_2 in a CPMG experiment against the natural logarithm of the pulse spacing—the data are from Fig. 9. The line represents Eq. (69).

delays of less than 100 μs, or spin-locking with fields corresponding to 10 kHz can heat the samples significantly. Recently, however, the method has proved useful in protein NMR. Several groups [97, 168–170] have been able to detect sparsely populated 'excited' states of proteins (conformations with higher energy than the most stable state).

Recently, there has been an elegant advance in this field. If we have a value for the rate from the T_2, dispersion, then we can also determine the square of the chemical shift difference, from Eq. (68), but not its sign. This is not important for a mutual exchange case, but for an unequally populated case (exchange with a 'hidden' higher energy conformation of a protein), the sign is very useful. If we can observe multiple quantum transitions and make careful measurements, we can also get the sign of the chemical shift difference [171], since the way that the exchange affects double- and zero-quantum transitions is different.

7. Exchange in the solid state

The basic principles of chemical exchange in solid-state NMR are much the same as for liquids, but the number of interactions that determine the frequencies of the individual sites is much larger. This is, perhaps, oversimplifying the still-expanding range of dynamic effects in solid-state NMR, but there are many similarities. Since chemical shieldings are often anisotropic, a simple molecular reorientation on a lattice site will cause a shift in frequency. Other effects, such as dipolar coupling or quadrupole interactions can give rise to similar effects. Perhaps, the most familiar example is the dramatic changes in the powder pattern of a deuterium nucleus when the molecule reorients [172–174]. Fig. 22 shows some simulations [175] of what happens to the spectrum when a static molecule starts to undergo two-fold flips. When the molecule reorients, then the deuterium quadrupole tensor goes from one orientation with respect to the magnetic field to another. For an isolated molecule undergoing two-fold flips, this would just be the exchange between two sites, each of which has the characteristic two-line spectrum of a spin-1 nucleus, but with different quadrupole splittings. The spectra in Fig. 22 are made up of these simple spectra, averaged over all possible orientations of the molecule. The powder average can be

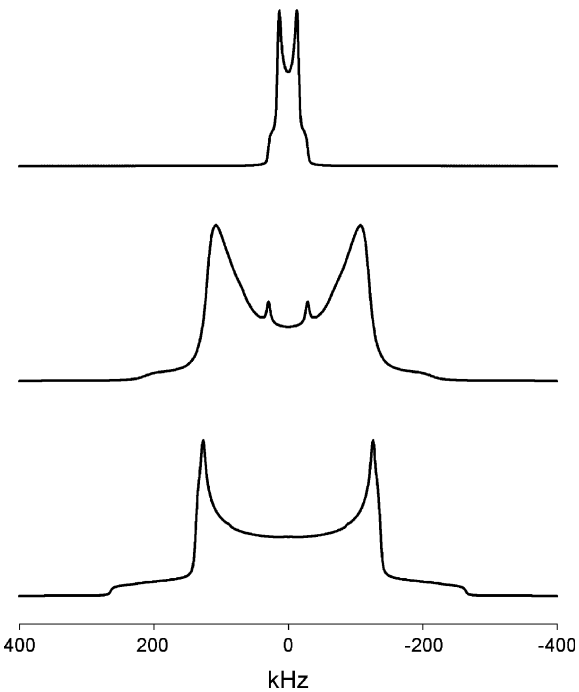

Fig. 22. Simulations of deuterium powder patterns for a single deuteron undergoing two-fold flips. The simulations were done using the program from Greenfield et al. [175].

efficiently done either using a tiling algorithm [176], or by using the less intuitive but more efficient Zaremba–Conroy–Wolfsberg method [177–180].

MAS imposes a further timescale on the spectrum. Fig. 11 has already shown what exchange will do to a pattern of spinning sidebands. The Hamiltonian of the system is now time-dependent, due to the sample rotation [181,182]. The exchange spectra can be simulated in a number of ways [183,184], but the method that fits the approach taken here is to use Floquet theory [31,32,185–187]. This approach is to expand the time-dependent Hamiltonian (or Liouvillian) into a set of Fourier components. The expanded problem is now time-independent, so the exchange takes place between the sets of Floquet states. The setup of the Floquet states is more complex, but the implementation of exchange is the same as in a liquid-state system.

Sidebands also show exchange effects if the exchange is relatively slow. Exchange will cause cross-peaks in a 2D spectrum [188,189], giving quite a sensitive test of slow exchange. If the sidebands are to be suppressed using the TOSS sequence [190], chemical exchange will start to destroy that suppression —sidebands will reappear even if the timing and pulses are exact [191]. Although the analogy between sidebands and sites is not a good one, the ODESSA experiment [192–194] has similarities to the slow-exchange, selective inversion experiment. In the ODESSA experiment, the intensities of the sidebands are perturbed from equilibrium, and we observe their return, as in liquids.

In the limit of fast spinning, when only the centre band remains, lineshape effects identical to those in liquids will be observable [195–205]. These spectra can be treated in the same way as in liquids.

8. Fitting exchange spectra

Once we have explained the general physical basis of the phenomena we have observed, we often want quantitative information on the rate of the process. This can be a relatively simple estimate, such as that determined at the coalescence temperature, Eq. (16), or from the ratio of a cross-peak to a diagonal peak in EXSY, Eq. (67). However, careful measurements are needed for precise estimates of thermodynamic quantities. The best way to do this is to model the spectra, then adjust the parameters of the model (including the rate) until a best fit is achieved. Modelling of spectra has been done from the early days of both computers and NMR [206]. One of the applications is the analysis of spectra [207–211], another is fitting the static lines themselves [212], and a third common application is chemical exchange [12, 36,122,213–215]. Another task is fitting the selective inversion data, in order to extract the rate [142, 147–150,155]. There are two parts to these problems: first, the calculation of the spectrum, and second, the variation of the parameters in some automatic way in order to achieve the best fit. Calculation of the spectrum is fairly easy—it is based on the diagonalization of the Hamiltonian for the static spectrum and the Liouvillian for the dynamic one. The more difficult problem is finding the best fit. In practice, we find fitting exchange spectra easier than static spectra. Because the lines are generally broad in dynamic NMR, the fitting often converges relatively easily. The many local minima that bedevil the fitting of complicated strongly coupled spectra seem to be much less of a problem in chemical exchange.

The best fit is usually defined by minimizing the sum of the squares of the differences between the observed data and the calculated model [216–218]. Parameters in the model are guessed, to begin with, then adjusted to improve the fit. There are two common approaches: the simplex algorithm [219], and the Marquardt approach [220,221]. Simplex is simple to implement, since partial derivatives are not needed, but it is inefficient. In spite of its slow speed, however, it seems quite reliable. The Marquardt approach (sometimes called Levenberg–Marquardt) [218] is much more efficient, but it requires evaluation of partial derivatives of the data with respect to the parameters. This may sound intimidating, but in practice with NMR data, it is straightforward. Let us consider the two-site equally populated exchange lineshape, and how to fit it [222].

Eq. (15) gives the lineshape, $s(\omega)$, for two sites, at frequencies (in rad s^{-1}) of $\pm\delta$, exchanging at a rate, k. If we remove some of the constants, this equation can be rewritten as

$$s(\omega) = \frac{k\delta^2}{(\omega^2 - \delta^2)^2 + 4k^2\omega^2}. \tag{71}$$

To fit an experimental spectrum, $f(\omega)$, to this equation, we must minimize the sum of the squares of the deviations between the experimental and the simulated lineshape [216,217]. This minimization must be done as a function of the parameters k and δ. It is common to call this sum of squares χ^2, given by

$$\chi^2(k,\delta) = \sum_{i=1}^{n} (f(\omega_i) - s(\omega_i))^2. \tag{72}$$

In this equation, the sum is used, since it assumed that the spectrum is represented as a series of n digitized points, at frequencies ω_i.

Close to the minimum of this function, small offsets of δ and k will change the simulation slightly such that:

$$\mathrm{d}(f(\omega_i) - s(\omega_i)) \approx \frac{\partial s}{\partial \delta}\mathrm{d}\delta + \frac{\partial s}{\partial k}\mathrm{d}k. \tag{73}$$

Therefore, χ^2 will be given by

$$\begin{aligned}\chi^2(k,\delta) \approx \sum_i \Bigg[&\left(\frac{\partial s}{\partial k}\right)^2 (\mathrm{d}k)^2 + 2\left(\frac{\partial s}{\partial k}\right)\left(\frac{\partial s}{\partial \delta}\right)\mathrm{d}k\,\mathrm{d}\delta \\ &+ \left(\frac{\partial s}{\partial \delta}\right)^2 (\mathrm{d}\delta)^2 \Bigg] \\ = (\mathrm{d}k)^2 &\sum_i \left(\frac{\partial s}{\partial k}\right)^2 + 2\,\mathrm{d}k\,\mathrm{d}\delta \sum_i \left(\frac{\partial s}{\partial k}\right)\left(\frac{\partial s}{\partial \delta}\right) \\ &+ (\mathrm{d}\delta)^2 \sum_i \left(\frac{\partial s}{\partial \delta}\right)^2. \end{aligned} \tag{74}$$

It is convenient to recast this as a matrix expression, defining a matrix, $\mathbf{A}$:

$$\mathbf{A} = \begin{pmatrix} \frac{\partial s(\omega_1)}{\partial k} & \frac{\partial s(\omega_1)}{\partial \delta} \\ \frac{\partial s(\omega_2)}{\partial k} & \frac{\partial s(\omega_2)}{\partial \delta} \\ \vdots & \vdots \\ \frac{\partial s(\omega_{n-1})}{\partial k} & \frac{\partial s(\omega_{n-1})}{\partial \delta} \\ \frac{\partial s(\omega_n)}{\partial k} & \frac{\partial s(\omega_n)}{\partial \delta} \end{pmatrix}. \tag{75}$$

This matrix has two columns, for the two variables, and n rows, since the partial derivatives are evaluated at each of the data points. The definition of this matrix allows us to write χ^2 as a quadratic form

$$\chi^2 = (\mathrm{d}k \;\; \mathrm{d}\delta)(\mathbf{A}^{\mathrm{tr}}\mathbf{A})\begin{pmatrix}\mathrm{d}k \\ \mathrm{d}\delta\end{pmatrix}, \tag{76}$$

in which $\mathbf{A}^{\mathrm{tr}}$ is the transpose of $\mathbf{A}$. The 2x2 matrix, $\mathbf{A}^{\mathrm{tr}}\mathbf{A}$, is important because it defines the shape of the χ^2 surface near the minimum and it is given by

$$\mathbf{A}^{\mathrm{tr}}\mathbf{A} = \begin{pmatrix} \sum\left(\frac{\partial s}{\partial k}\right)^2 & \sum\left(\frac{\partial s}{\partial k}\right)\sum\left(\frac{\partial s}{\partial \delta}\right) \\ \sum\left(\frac{\partial s}{\partial k}\right)\sum\left(\frac{\partial s}{\partial \delta}\right) & \sum\left(\frac{\partial s}{\partial \delta}\right)^2 \end{pmatrix}. \tag{77}$$

This quadratic form depends on the partial derivatives in Eq. (77). Some calculus, applied to equation, gives the partial derivatives

$$\begin{aligned}\frac{\partial s}{\partial k} &= \frac{4\delta^2(\omega^4 + \delta^4 - 4k^2\omega^2 - 2\delta^2\omega^2)}{((\omega^2 - \delta^2)^2 + 4k^2\omega^2)^2}, \\ \frac{\partial s}{\partial \delta} &= \frac{8k\delta(\omega^4 - \delta^4 + 4k^2\omega^2)}{((\omega^2 - \delta^2)^2 + 4k^2\omega^2)^2}. \end{aligned} \tag{78}$$

Figs. 23 and 24 show calculated surfaces of χ^2 for two sets of parameters, one in which the rate is below coalescence, and one at which it is at coalescence. Fig. 25 shows an experimental χ^2 surface for the data in Fig. 1, at a rate corresponding to Fig. 23. The axes are the difference of the rate from its true value, and the difference between the frequency difference (in rad s^{-1}) of the two sites and its true value. The surface goes to zero at the middle of the plot. These figures illustrate several points. First, the ellipsoid is elongated and tilted with respect to the parameter axes. This is an indication of the correlation between the frequency difference and the rate—similar spectra can be calculated with a range of these parameters. As the spectrum approaches and passes coalescence, the correlation gets stronger, until in the fast exchange limit, we can only determine their ratio. An independent measure of the frequency difference is needed, as discussed above. The increase of the tilt and elongation between Figs. 23 and 24 is the graphical indication of this effect.

It is sometimes said that the spectrum is most sensitive to the rate at the coalescence point. This is arguably true, provided an accurate value of the frequency difference is available. However, chemical shifts and their differences are usually

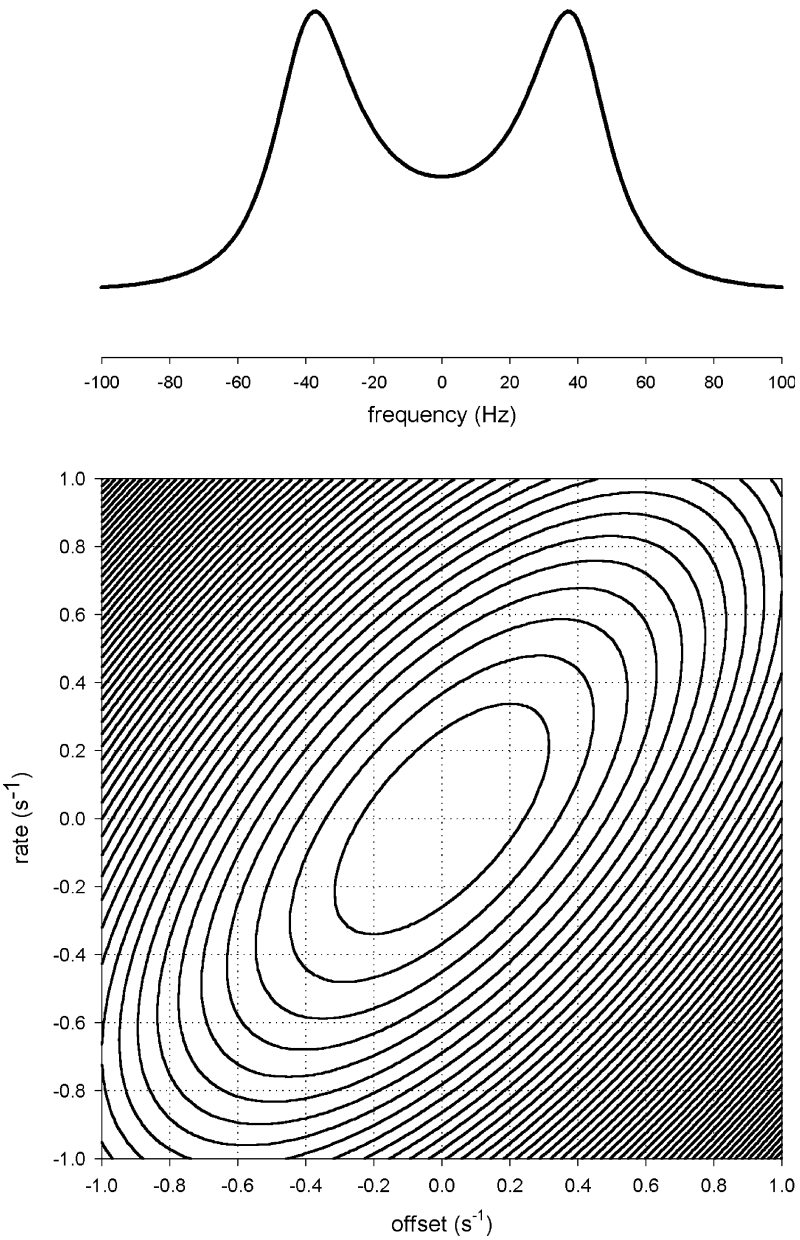

Fig. 23. Contour plot of the goodness of fit, χ^2, as a function of the rate and the offset from the ideal frequency difference, in the fitting of the exchange lineshape at the top of the plot. The contours follow Eq. (77).

temperature-dependent (Fig. 26), so some independent check on the frequency separation of the sites is extremely useful. It is our opinion that the best estimates of a rate come from spectra just below coalescence, such as in Fig. 23.

The minimum in the χ^2 surface can be found in a number of ways, beyond plotting it out as in Fig. 25. The easiest to implement is the simplex method, which simply requires evaluation of χ^2 at $(n+1)$ sets of parameters, if n parameters are being optimized

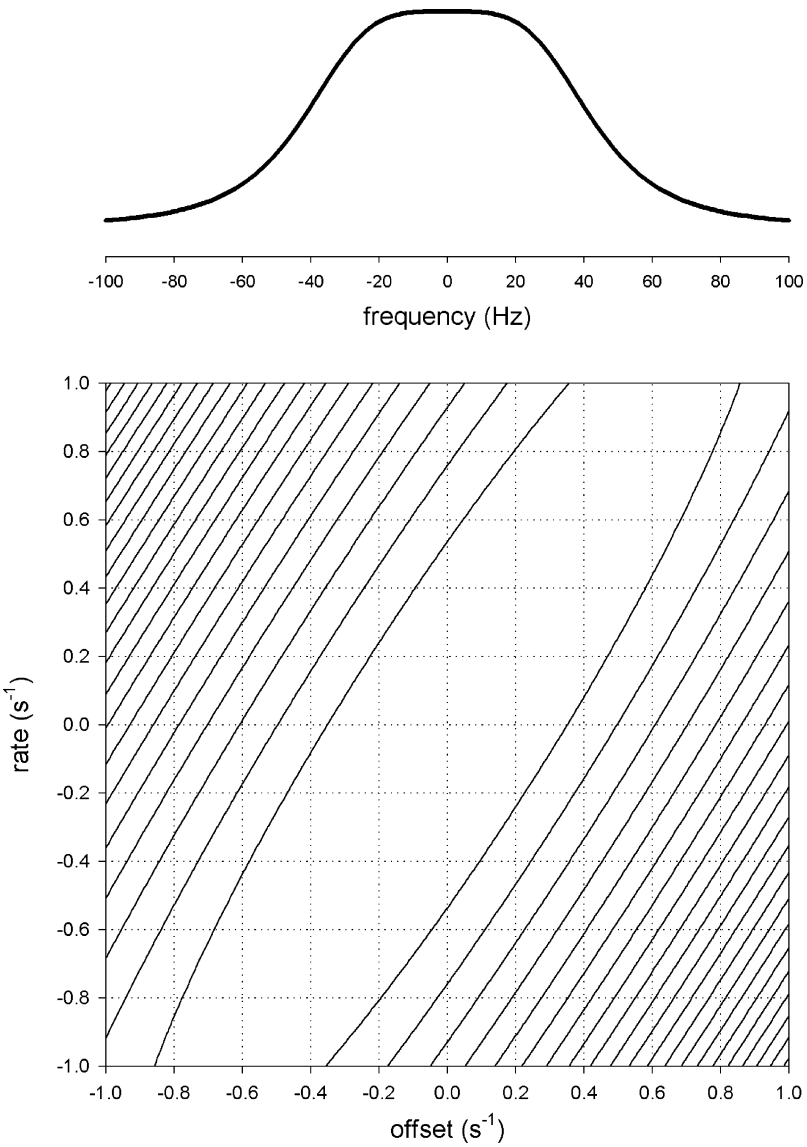

Fig. 24. Contour plot of the goodness of fit, χ^2, as a function of the rate and the offset from the ideal frequency difference, for a spectrum at coalescence.

[218,219]. This is the basis of the MEXICO suite of programs that we have written. It has proved to be quite reliable, if somewhat inefficient (50–100 iterations needed). Binsch and Stephenson's durable and justly famous program DNMR5 uses a derivative-based approach, related to Marquardt's method [218]. The advantage of this is that the convergence is faster, but each step requires the calculation of partial derivatives of each spectral point with respect to each parameter. This sounds daunting, since it requires propagating a partial derivative through an eigenvalue calculation [124], but it should not be. The results are very similar to perturbation theory applied to eigenvalues and eigenvectors in quantum mechanics. In the derivative-based approach, there are fewer iterations, but each iteration is slower. Our

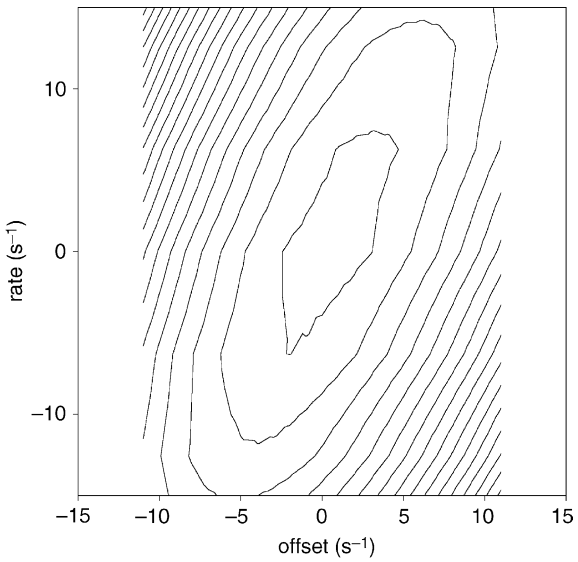

Fig. 25. Contour plot of the goodness of fit, χ^2, using experimental data from Fig. 1 and parameters similar to Fig. 23.

experience is that the performance of simplex methods and derivative methods is roughly similar. Fig. 27 shows the type of results that are possible.

How accurate are the rates obtained from such fits? They are achieved by varying frequencies and rates and other parameters until a best fit is achieved. How do we define the error in a single parameter? There is no definitive answer to this question. If a derivative-based method is used, the variance–covariance matrix is automatically available as part of the calculation [216,217]. The variance of a single parameter is obtained from the diagonal element of the matrix. In Fig. 23, this corresponds to an intersection of the appropriate contour with the parameter axis. However, there is usually substantial covariance, shown by the tilt and elongation of the contours in Figs. 23 and 24. It can be argued that the extreme values of the ellipses, not their intersections with the axes, should be used [217]. Another approach, taken in LAOCOON and some other programs [207], is to diagonalize the covariance matrix, so that you have linear combinations of parameters that are statistically independent. Again, this is not a totally satisfactory definition of the error of a single parameter.

Perhaps the best way to estimate the error in the rate is to use a method sometimes called 'profiling' [217]. If you are varying a rate, plus a number of chemical shifts and other parameters, then first find a global minimum in the parameter hyper-surface. Then, fix the rate at some value slightly different from the optimum and refit the spectrum, varying all the other parameters. The fit will be worse, i.e. the value of χ^2 will be above its global minimum. This process is then repeated for a series of rates that deviate more and more from the optimum, and the value of χ^2 is plotted. When this value of χ^2 becomes 'too big', this then gives an estimate of the error. The question then becomes, what is too big? The answer involves the F statistic, and for simple situations such as selective inversion experiments in slow exchange (see below), it seems to give reasonable answers. For spectra [223], the question of what is too big is less clear.

Selective inversion data, such as in Fig. 16, are fitted in a similar way. Muhandiram and McClung

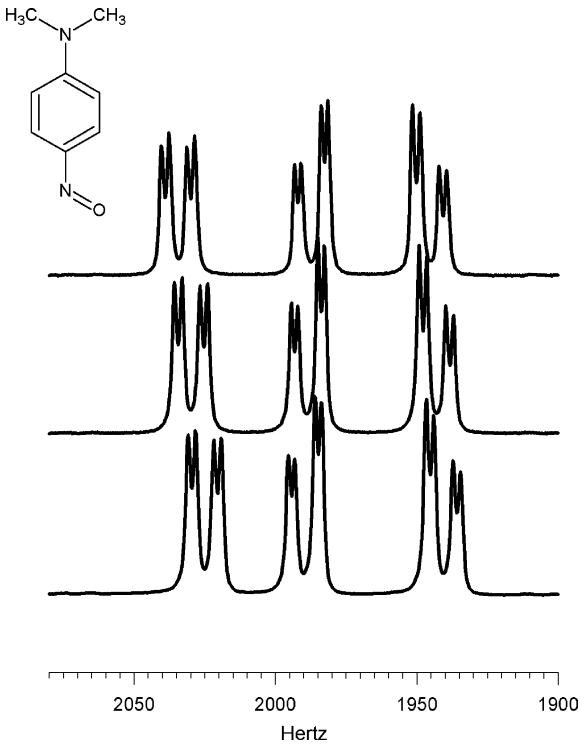

Fig. 26. Illustration of the temperature dependence of chemical shifts of the three low-frequency aromatic protons (see Fig. 2) in *p*-nitrosodimethylaniline (structure shown in the figure). The spectra (from bottom to top) represent 193, 213, and 233 K. Data like these are important in order to extrapolate frequency differences to the region near coalescence.

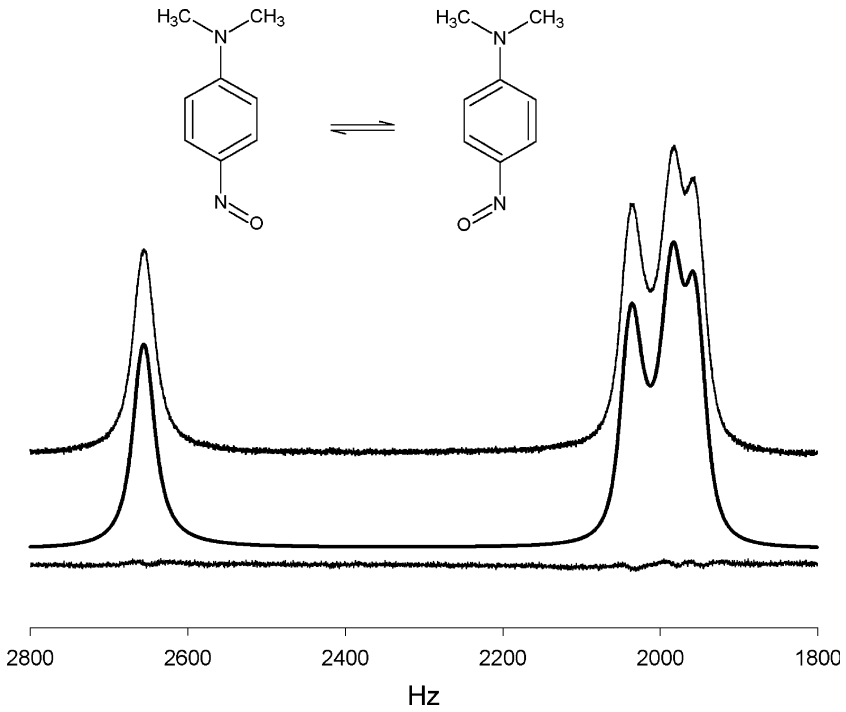

Fig. 27. Experimental (top) and calculated (middle trace) exchange lineshape for *p*-nitrosodimethylaniline. The calculated spectrum was fitted by the iterative version of the MEXICO program, and the bottom line represents the difference between the fitted and the experimental lineshapes.

provided [147] formulae for partial derivatives in an eigenvalue problem, to which we made a small correction [155]. A related problem is the use of NOE constraints in protein structure calculations [224]. In this case, the profiling works well [150], but indicates that the error estimate obtained this way is significantly higher than the value from the diagonal element of the variance–covariance matrix.

With good spectra, either lineshapes or selective inversion experiments, we feel that rates can be measured with realistic errors of a few percent. In fast exchange spectra, it is more difficult to estimate an error, since there are many parameters and relatively little data. However, consistency with numbers at slower rates, as in Fig. 13, gives confidence in all the data. If possible, multiple techniques should be used.

9. Conclusions

We have seen several different manifestations of chemical exchange in NMR, but there are many more. However, we hope we have shown that they are all described in a similar approach. For each site, there is a Liouvillian (a superoperator, defined by the commutator with the Hamiltonian), which defines the static spectrum in that site. This can be a simple frequency, as in the case of uncoupled exchange, or a full Liouvillian in Floquet space for a MAS spectrum. The Liouvillians for the sites are connected by the exchange matrix, and the final spectrum is defined by the composite Liouvillian.

In practice, this means that systems in slow exchange with well-defined sites show coupled spin–lattice relaxation. This leads to cross-peaks in an EXSY spectrum, or multi-exponential decay in a selective inversion experiment. For systems in intermediate exchange, there are again multiple exponentials, but now they contain both oscillatory and decaying terms. These exponentials are the transitions we see in the spectrum. The unusual lineshapes seen in intermediate exchange arise because the individual transitions are quite strongly perturbed in frequency, intensity, phase and

linewidth. Instead of the familiar frequency and transition probability, we now have complex values with real and imaginary parts. An exchange lineshape is very little different from a static spectrum.

Chemical exchange effects are present in many of the NMR spectra we measure. With modern spectrometers, clear theory, fast computers and good software, the dynamics can be analyzed quite easily. Even if there are already a lot of dimensions to NMR, exchange adds another one.

Acknowledgements

Including a list of all the people who have helped in doing this work would almost double the length of the manuscript, so I will have to thank them as a group rather than individually. Financial support for all this work was provided by the Natural Sciences and Engineering Research Council of Canada (NSERC).

References

[1] H.S. Gutowsky, C.H. Holm, J. Chem. Phys. 25 (1956) 1228.
[2] H.M. McConnell, J. Chem. Phys. 28 (1958) 430.
[3] L.M. Jackman, F.A. Cotton, Dynamic Nuclear Magnetic Resonance Spectroscopy, Academic Press, New York, 1975.
[4] J. Sandstrom, Dynamic NMR Spectroscopy, Academic Press, London, 1982.
[5] J.I. Kaplan, G. Fraenkel, NMR of Chemically Exchanging Systems, Academic Press, New York, 1980.
[6] J.J. Delpeuch (Ed.), Dynamics of Solutions and Fluid Mixtures by NMR, Wiley, Chichester, 1995.
[7] R. Tycko (Ed.), Nuclear Magnetic Resonance Probes of Molecular Dynamics, Kluwer Academic Publishers, Boston, 1994.
[8] C.S. Johnson, Adv. Magn. Reson. 1 (1965) 33.
[9] R.M. Lynden-Bell, Prog. Nucl. Magn. Reson. Spectrosc. 2 (1967) 163.
[10] L.W. Reeves, Adv. Phys. Org. Chem. 3 (1965) 187.
[11] J.P. Jesson, P. Meakin, Acc. Chem. Res. 6 (1973) 269.
[12] G. Binsch, H. Kessler, Angew. Chem. Int. Ed. Engl. 19 (1980) 411.
[13] K.G. Orrell, in: D.M. Grant, R.K. Harris (Eds.), The Encyclopedia of NMR, Wiley, Chichester, 1996, p. 4850.
[14] W.E. Stewart, T.H. Siddall, Chem. Rev. 70 (1970) 517.
[15] T. Fauconnier, A.D. Bain, P. Hazendonk, R.A. Bell, C.J.L. Lock, Can. J. Chem. 76 (1998) 426.
[16] P.D. Buckley, A.R. Furness, K.W. Jolley, D.N. Pinder, Aust. J. Chem. 27 (1974) 21.
[17] A.R. Furness, P.D. Buckley, K.W. Jolley, Aust. J. Chem. 28 (1975) 2303.
[18] K.G. Orrell, A.G. Osborne, V. Sik, M.W. DaSilva, Polyhedron 14 (1995) 2797.
[19] M.K. Chung, G. Ferguson, V. Robertson, M. Schlaf, Can. J. Chem. 79 (2001) 949.
[20] W.G. Schneider, L.W. Reeves, Ann. N. Y. Acad. Sci. 70 (1958) 858.
[21] D.R. Muhandiram, R.E.D. McClung, J. Magn. Reson. 76 (1988) 121.
[22] M. Helgstrand, T. Hard, P. Allard, J. Biomol. NMR 18 (2000) 49.
[23] V.J. Robinson, A.D. Bain, Magn. Reson. Chem. 31 (1993) 865.
[24] E.J. Cabrita, S. Berger, Magn. Reson. Chem. 40 (2002) S122–S127.
[25] T.T. Nakashima, R.E.D. McClung, G. Kotovych, J. Magn. Reson. 133 (1999) 222.
[26] R.E.D. McClung, T.T. Nakashima, H. Yamamoto, G. Kotovych, Can. J. Chem. 77 (1999) 1728.
[27] S. Forsen, R.A. Hoffman, J. Chem. Phys. 40 (1964) 1189.
[28] J. Jeener, B.H. Meier, P. Bachmann, R.R. Ernst, J. Chem. Phys. 71 (1979) 4546.
[29] P.A. Duspara, C.F. Matta, S.I. Jenkins, P.H.M. Harrison, Org. Lett. 3 (2001) 495.
[30] A.D. Bain, R.A. Bell, D.A. Fletcher, P. Hazendonk, R.B. Maharajh, S. Rigby, J.F. Valliant, J. Chem. Soc. Perkin Trans. 2 (1999) 1447.
[31] S. Vega, in: R. Tycko (Ed.), Nuclear Magnetic Resonance Probes of Molecular Dynamics, Kluwer Academic Publishers, Boston, 1994, p. 155.
[32] P. Hazendonk, A.D. Bain, H. Grondey, P.H.M. Harrison, R.S. Dumont, J. Magn. Reson. 146 (2000) 33.
[33] H.S. Gutowsky, D.W. McCall, C.P. Slichter, J. Chem. Phys. 21 (1953) 279.
[34] R.K. Gupta, T.P. Pitner, R.E. Wasylishen, J. Magn. Reson. 13 (1974) 383.
[35] G.P. Moss, Pure Appl. Chem. 68 (1996) 2193.
[36] S.O. Chan, L.W. Reeves, J. Am. Chem. Soc. 95 (1973) 670.
[37] S.O. Chan, L.W. Reeves, J. Am. Chem. Soc. 95 (1973) 673.
[38] S.O. Chan, L.W. Reeves, Inorg. Chem. 12 (1973) 1704.
[39] E. Vallazza, A.D. Bain, T.W. Swaddle, Can. J. Chem. 76 (1998) 183.
[40] L.W. Reeves, K.N. Shaw, Can. J. Chem. 48 (1970) 3641.
[41] J.R. Zimmerman, W.E. Brittin, J. Phys. Chem. 61 (1957) 1328.
[42] A.A. Istratov, O.F. Vyvenko, Rev. Sci. Instrum. 70 (1999) 1233.
[43] G.R. Moran, D.D. Bellamy, J. Sykes, F.S. Prato, Magn. Reson. Med. (2003) in press.
[44] S.D. Beyea, B.J. Balcom, T.W. Bremner, R.L. Armstrong, P.E. Grattan-Bellew, J. Am. Ceram. Soc. 86 (2003) 800.
[45] W. Nordhoy, H.W. Anthionsen, M. Bruvold, P. Jynge, J. Krane, H. Brurok, NMR Biomed. 16 (2003) 82.
[46] C. Plata-Iglesias, D.M. Corsi, L. VanderElst, R.N. Muller, D. Imbert, J.C.G. Bunzli, E. Toth, T. Maschmeyer, J.A. Peters, J. Chem. Soc., Dalton Trans. (2003) 727.

[47] H. Kessler, Angew. Chem. Int. Ed. Engl. 9 (1970) 219.
[48] L.J. Farrugia, J. Chem. Soc., Dalton Trans. (1997) 1783.
[49] C.B. LeMaster, Prog. Nucl. Magn. Reson. Spectrosc. 31 (1997) 119.
[50] K.G. Orrell, V. Sik, Annu. Rep. NMR Spectrosc. 19 (1987) 79.
[51] K.G. Orrell, Annu. Rep. NMR Spectrosc. 37 (1999) 1.
[52] K.G. Orrell, V. Sik, Annu. Rep. NMR Spectrosc. 27 (1993) 103.
[53] M. Pons, O. Millet, Prog. Nucl. Magn. Reson. Spectrosc. 38 (2001) 267.
[54] L. Fielding, Tetrahedron 56 (2000) 6151.
[55] R.Y. Dong, Prog. Nucl. Magn. Reson. Spectrosc. 41 (2002) 115.
[56] E.R. Johnston, Concepts Magn. Reson. 7 (1995) 219.
[57] G. Aguirre, R. Somanathan, L. Hellberg, T. Dwyer, R. North, Magn. Reson. Chem. 41 (2003) 131.
[58] K.C. Brown, R.L. Tyson, J.A. Weil, J. Chem. Ed. 75 (1998) 1632.
[59] T. Dwyer, J.E. Norman, P.G. Jasien, J. Chem. Ed. 75 (1998) 1635.
[60] R.A. Bragg, J. Clayden, G.A. Morris, J.H. Pink, Chem. Eur. J. 8 (2002) 1279.
[61] F.J. Monlien, L. Helm, A. Abou-Hamdan, A.E. Merbach, Inorg. Chem. 41 (2002) 1717.
[62] J.J. Skalicky, J.L. Mills, S. Sharma, T. Szyperski, J. Am. Chem. Soc. 123 (2001) 388.
[63] P.S. Sidhu, G.D. Enright, J.A. Ripmeester, G.H. Penner, J. Phys. Chem. 106B (2002) 8569.
[64] U. Gross, D. Pfeifer, J. Fluorine Chem. 113 (2002) 17.
[65] S.E. Boiadjiev, D.A. Lightner, Monatshefte Chem. 133 (2002) 1469.
[66] C. Wolf, L. Pranatharthiharan, R.B. Ramagosa, Tetrahedron Lett. 43 (2002) 8563.
[67] S.P. Babilov, D.A. Mainichev, J. Inclusion Phenom. Macrocycl. Chem. 43 (2002) 187.
[68] M.B. Garcia, S. Grilli, L. Lunazzi, A. Mazzanti, L.R. Orelli, Eur. J. Org. Chem. (2002) 4018.
[69] R.T. Boere, J.D. Masuda, Can. J. Chem. 80 (2002) 1607.
[70] L. Scaglioni, S. Mazzini, R. Mondelli, L. Merlini, E. Ragg, G. Nasini, J. Chem. Soc. Perkin Trans. 2 (2001) 2276.
[71] J.S. Lomas, A. Adenier, J. Chem. Soc. Perkin Trans. 2 (2002) 1264.
[72] M.E. Amato, G.A. Carriedo, F.J. Garcia Alonso, J.L. Garcia-Alvarez, G.M. Lombardo, G.C. Pappalardo, J. Chem. Soc., Dalton Trans. (2002) 3047.
[73] R. Baldwin, M.A. Bennett, D.C.R. Hockless, P. Pertici, A. Verrazzani, G.U. Barretta, F. Marchetti, P. Salvadori, J. Chem. Soc., Dalton Trans. (2002) 4488.
[74] I. Yavari, M. Adib, F. Jahani-Moghaddam, H.R. Bijanzadeh, Tetrahedron 58 (2002) 6901.
[75] A. Bongini, G. Barbarella, L. Favaretto, G. Sotgiu, M. Zambianchi, D. Casarini, Tetrahedron 58 (2002) 10151.
[76] L.J. Ackerman, M.L.H. Green, J.C. Green, J.E. Bercaw, Organometallics 22 (2003) 188.
[77] S.G. Shore, E.J.M. Hamilton, A.N. Bridges, J. Bausch, J.A. Krause-Bauer, D. Dou, J. Liu, S. Liu, B. Du, H. Hall, E.A. Meyers, K.E. Vermillion, Inorg. Chem. 42 (2003) 1175.
[78] H.F. Klein, R. Beck, O. Hetche, Eur. J. Inorg. Chem. (2003) 232.
[79] D. Casarini, C. Rosini, S. Grilli, L. Lunazzi, A. Mazzanti, J. Org. Chem. 68 (2003) 1815.
[80] S. Braverman, Y. Zafrani, H.E. Gottlieb, J. Org. Chem. 67 (2002) 3277.
[81] I. Arnason, A. Kvaran, S. Jonsdottir, P.I. Gudnason, H. Oberhammer, J. Org. Chem. 67 (2002) 3827.
[82] M. Garcia-Valverde, R. Pascual, T. Torroba, Org. Lett. 5 (2003) 929.
[83] B. Birdsall, V.I. Polshakov, J. Feeney, Biochemistry 39 (2000) 9819.
[84] F.J. Monlien, L. Helm, A. Abou-Hamdan, A.E. Merbach, Inorg. Chim. Acta 331 (2002) 257.
[85] D. Schott, C.J. Sleigh, J.P. Lowe, S.B. Duckett, R.J. Mawby, Inorg. Chem. 41 (2002) 2960.
[86] J.C. Rodrigues, P.A. Jennings, G. Melacini, J. Am. Chem. Soc. 124 (2002) 6240.
[87] V.P. Denisov, B. Halle, J. Am. Chem. Soc. 124 (2002) 10264.
[88] D. Uhrin, A.V. Krishna Prasad, J.R. Brisson, D.R. Bundle, Can. J. Chem. 80 (2002) 904.
[89] F.A.A. Mulder, N.R. Skrynnikov, B. Hon, F.W. Dahlquist, L.E. Kay, J. Am. Chem. Soc. 123 (2001) 967.
[90] F.A.A. Mulder, A. Mittermaier, B. Hon, F.W. Dahlquist, L.E. Kay, Nature Struct. Biol. 8 (2001) 932.
[91] F. Taube, I. Andersson, I. Toth, A. Bodor, O.W. Howarth, L. Pettersson, J. Chem. Soc., Dalton Trans. (2002) 4451.
[92] D.M. Korzhnev, B.G. Karlsson, V.Y. Orekhov, M. Billeter, Protein Sci. 12 (2003) 56.
[93] N. Biris, A. Stavrakoudis, A.S. Politou, E. Mikros, M. Sakarellos-Daitsiotis, C. Sakarellos, V. Tsikaris, Biopolymers 69 (2003) 72.
[94] C.A. Fyfe, A.C. Diaz, J. Phys. Chem. 106B (2002) 2261.
[95] L.E. Harrington, J.F. Britten, D.W. Hughes, A.D. Bain, J.Y. Thepot, M.J. McGlinchey, J. Organomet. Chem. 656 (2002) 243.
[96] J.K. Rubach, B.V. Plapp, Biochemistry 41 (2002) 15770.
[97] O. Trott, A.G. Palmer, J. Magn. Reson. 154 (2002) 157.
[98] F. Wehrmann, J. Albrecht, E. Gedat, G.J. Kubas, J. Eckert, H.H. Limbach, G. Buntkowsky, J. Phys. Chem. 106 (2002) 2855.
[99] N. Vasdev, B.E. Pointner, R. Chirakal, G.J. Schrobilgen, J. Am. Chem. Soc. 124 (2002) 12863.
[100] M. Hoang, G. Mladenova, A.C. Hopkinson, J. Ramnauth, E. Lee-Ruff, Magn. Reson. Chem. 39 (2001) 294.
[101] H.E. Birkett, R.K. Harris, P. Hodgkinson, K. Carr, M.H. Charlton, J.R. Cherryman, A.M. Chippendale, R.P. Glover, Magn. Reson. Chem. 38 (2000) 504.
[102] P.S. Denkova, V.S. Dimitrov, Magn. Reson. Chem. 37 (1999) 637.
[103] N.R. Skrynnikov, R.R. Ernst, J. Magn. Reson. 137 (1999) 276.
[104] P.J. Heard, P.M. King, A.D. Bain, P. Hazendonk, D.A. Tocher, J. Chem. Soc., Dalton Trans. (1999) 4495.

[105] S. Beyreuther, A. Frick, J. Hunger, G. Huttner, B. Antelmann, P. Schober, R. Soltek, Eur. J. Inorg. Chem. (2000) 597.
[106] A.J. Preston, G. Fraenkel, A. Chow, J.C. Gallucci, J.R. Parquette, J. Org. Chem. 68 (2003) 22.
[107] J.M. Veauthier, A. Chow, G. Fraenkel, S.J. Geib, N.J. Cooper, Organometallics 19 (2000) 3942.
[108] K.J. Laidler, Chemical Kinetics, McGraw-Hill, New York, 1965.
[109] A.D. Bain, G.J. Duns, F. Rathgeb, J. Vanderkloet, J. Phys. Chem. 99 (1995) 17338.
[110] C.T.G. Knight, A.E. Merbach, Inorg. Chem. 24 (1985) 576.
[111] T. Drakenberg, R.E. Carter, Org. Magn. Reson. 7 (1975) 307.
[112] A.J. Wand, Nature Struct. Biol. 8 (2001) 926.
[113] D.A. Benefraim, R. Aradyellin, J. Chem. Soc. Perkin Trans. 2 (1994) 853.
[114] U. Berg, U. Sjostrand, Org. Magn. Reson. 11 (1978) 555.
[115] C. Cox, T. Lectka, J. Org. Chem. 63 (1998) 2426.
[116] V.S. Dimitrov, N.G. Vassilev, Magn. Reson. Chem. 33 (1995) 739.
[117] C. Dreir, L. Henriksen, S. Karlsson, J. Sandstrom, Acta Chem. Scand. B 32 (1978) 282.
[118] M.L. Martin, F. Mabon, M. Trierweiler, J. Phys. Chem. 85 (1981) 76.
[119] A.D. Bain, P. Hazendonk, J. Phys. Chem. 101A (1997) 7182.
[120] C. Suarez, E.J. Nicholas, M.R. Bowman, J. Phys. Chem. 107A (2003) 3024.
[121] J.I. Kaplan, J. Chem. Phys. 29 (1958) 462.
[122] G. Binsch, J. Am. Chem. Soc. 91 (1969) 1304.
[123] C. Moler, C.F. van Loan, SIAM Rev. 20 (1978) 801.
[124] J.H. Wilkinson, The Algebraic Eigenvalue Problem, Clarendon Press, Oxford, 1965.
[125] R.R. Ernst, G. Bodenhausen, A. Wokaun, Principles of Nuclear Magnetic Resonance in One and Two Dimensions, Clarendon Press, Oxford, 1987.
[126] C.P. Slichter, Principles of Magnetic Resonance, Springer, Berlin, 1989.
[127] U. Fano, Rev. Mod. Phys. 29 (1957) 74.
[128] U. Fano, in: E.R. Caianiello (Ed.), Lectures on the Many Body Problem, vol. 2, Academic Press, New York, 1964, p. 217.
[129] C.N. Banwell, H. Primas, Mol. Phys. 6 (1963) 225.
[130] J. Jeener, Adv. Magn. Reson. 10 (1982) 1.
[131] A.D. Bain, Prog. Nucl. Magn. Reson. Spectrosc. 20 (1988) 295.
[132] A.D. Bain, G.J. Duns, Can. J. Chem. 74 (1996) 819.
[133] R. Kubo, J. Phys. Soc. Jpn 9 (1954) 935.
[134] R.A. Sack, Mol. Phys. 1 (1958) 163.
[135] J.I. Kaplan, G. Fraenkel, J. Am. Chem. Soc. 94 (1972) 2907.
[136] J.E. Anderson, J.E.T. Corrie, J. Chem. Soc. Perkin Trans. 2 (1992) 1027.
[137] A.D. Bain, D.A. Fletcher, P. Hazendonk, Concepts Magn. Reson. 10 (1998) 85.
[138] A.D. Bain, J. Magn. Reson. 37 (1980) 209.
[139] A.D. Bain, J. Magn. Reson. 39 (1980) 335.
[140] S. Alexander, J. Chem. Phys. 37 (1962) 967.
[141] C.L. Perrin, J. Magn. Reson. 82 (1989) 619.
[142] A.D. Bain, J.A. Cramer, J. Phys. Chem. 97 (1993) 2884.
[143] K.G. Orrell, V. Sik, D. Stephenson, Prog. Nucl. Magn. Reson. Spectrosc. 22 (1990) 141.
[144] C.L. Perrin, T. Dwyer, Chem. Rev. 90 (1990) 935.
[145] B.E. Mann, J. Magn. Reson. 21 (1976) 17.
[146] M. Grassi, B.E. Mann, B.T. Pickup, C.M. Spencer, J. Magn. Reson. 69 (1986) 92.
[147] D.R. Muhandiram, R.E.D. McClung, J. Magn. Reson. 71 (1987) 187.
[148] R.E.D. McClung, G.H.M. Aarts, J. Magn. Reson. 115A (1995) 145.
[149] A.D. Bain, J.A. Cramer, J. Magn. Reson. 103A (1993) 217.
[150] A.D. Bain, J.A. Cramer, J. Magn. Reson. 118A (1996) 21.
[151] S. Schäublin, A. Höhener, R.R. Ernst, J. Magn. Reson. 13 (1974) 196.
[152] A.D. Bain, J.S. Martin, J. Magn. Reson. 29 (1978) 125.
[153] A.D. Bain, J.S. Martin, J. Magn. Reson. 29 (1978) 137.
[154] R.E.D. McClung, N.R. Krishna, J. Magn. Reson. 29 (1978) 573.
[155] A.D. Bain, D.A. Fletcher, Mol. Phys. 95 (1998) 1091.
[156] A.D. Bain, W.P.Y. Ho, J.S. Martin, J. Magn. Reson. 43 (1981) 328.
[157] A.D. Bain, G.J. Duns, J. Magn. Reson. 109A (1994) 56.
[158] R.L. Vold, R.R. Vold, H.E. Simon, J. Magn. Reson. 11 (1973) 283.
[159] A. Allerhand, H.S. Gutowsky, J. Chem. Phys. 41 (1964) 2115.
[160] A. Allerhand, H.S. Gutowsky, J. Chem. Phys. 42 (1965) 1587.
[161] A. Allerhand, H.S. Gutowsky, J. Chem. Phys. 42 (1965) 4203.
[162] C. Deverell, R.E. Morgan, J.H. Strange, Mol. Phys. 18 (1970) 553.
[163] J.P. Carver, R.E. Richards, J. Magn. Reson. 6 (1972) 89.
[164] P. Laszlo, Prog. Nucl. Magn. Reson. Spectrosc. 13 (1980) 257.
[165] M.A.K. Williams, T.K. Halstead, Mol. Phys. 93 (1998) 609.
[166] B.P. Hills, Mol. Phys. 76 (1992) 489.
[167] S. Chopra, R.E.D. McClung, R.B. Jordan, J. Magn. Reson. 59 (1984) 361.
[168] M. Akke, A.G. Palmer, J. Am. Chem. Soc. 118 (1996) 911.
[169] N.R. Skrynnikov, F.A.A. Mulder, B. Hon, F.W. Dahlquist, L.E. Kay, J. Am. Chem. Soc. (2001).
[170] M. Akke, Curr. Opin. Struct. Biol. 12 (2002) 642.
[171] N.R. Skrynnikov, F.W. Dahlquist, L.E. Kay, J. Am. Chem. Soc. 124 (2002) 12352.
[172] O. Pschorr, H.W. Spiess, J. Magn. Reson. 39 (1980) 217.
[173] R.R. Vold, R.L. Vold, Adv. Magn. Opt. Reson. 16 (1991) 85.
[174] R.R. Vold, in: R. Tycko (Ed.), Nuclear Magnetic Resonance Probes of Molecular Dynamics, Kluwer Academic Publishers, Boston, 1994, p. 27.
[175] M.S. Greenfield, A.D. Ronemus, R.L. Vold, R.R. Vold, P.D. Ellis, T.E. Raidy, J. Magn. Reson. 72 (1987) 89.
[176] D.W. Alderman, M.S. Solum, D.M. Grant, J. Chem. Phys. 84 (1986) 3717.

[177] S.C. Zaremba, Ann. Mat. Pura Appl. 4–73 (1966) 293.
[178] H. Conroy, J. Chem. Phys. 47 (1967) 5307.
[179] P. Hodgkinson, L. Emsley, Prog. Nucl. Magn. Reson. Spectrosc. 36 (2000) 201.
[180] V.B. Cheng, H.H. Suzukawa, M. Wolfsberg, J. Chem. Phys. 59 (1973) 3992.
[181] J. Herzfeld, A.E. Berger, J. Chem. Phys. 73 (1980) 6021.
[182] M.M. Maricq, J.S. Waugh, J. Chem. Phys. 70 (1978) 3300.
[183] A. Schmidt, R.G. Griffin, D.P. Raleigh, J.E. Roberts, S.O. Smith, S. Vega, J. Chem. Phys. 85 (1986) 4248.
[184] J.R. Long, B.Q. Sun, A. Bowen, R.G. Griffin, J. Am. Chem. Soc. 116 (1994) 11950.
[185] A. Schmidt, S. Vega, Isr. J. Chem. 32 (1992) 215.
[186] G.J. Boender, S. Vega, H.J.M. De Groot, Mol. Phys. 95 (1998) 921.
[187] A.D. Bain, R.S. Dumont, Concepts Magn. Reson. 13 (2001) 159.
[188] A.F. De Jong, A.P.M. Kentgens, W.S. Veeman, Chem. Phys. Lett. 109 (1984) 337.
[189] A.P.M. Kentgens, E. deBoer, W.S. Veeman, J. Chem. Phys. 87 (1987) 6859.
[190] W.T. Dixon, J. Chem. Phys. 77 (1982) 1800.
[191] Y. Yang, M. Schuster, B. Blumich, H.W. Spiess, Chem. Phys. Lett. 139 (1987) 239.
[192] Z. Luz, P. Tekely, D. Reichert, Prog. Nucl. Magn. Reson. Spectrosc. 41 (2002) 83.
[193] C. Jäger, D. Reichert, H. Zimmermann, T. Sen, R. Poupko, Z. Luz, J. Magn. Reson. 153 (2001) 227.
[194] D. Reichert, H. Zimmermann, P. Tekely, R. Poupko, Z. Luz, J. Magn. Reson. 125 (1997) 245.
[195] J.R. Lyerla, C.S. Yannoni, C.A. Fyfe, Acc. Chem. Res. 15 (1982) 208.
[196] F.G. Riddell, M. Rogerson, Magn. Reson. Chem. 35 (1997) 333.
[197] F.G. Riddell, K.S. Cameron, S.A. Holmes, J.H. Strange, J. Am. Chem. Soc. 119 (1997) 7555.
[198] D.A. Fletcher, B.G. Gowenlock, K.G. Orrell, V. Sik, Magn. Reson. Chem. 33 (1995) 561.
[199] D.A. Fletcher, B.G. Gowenlock, K.G. Orrell, V. Sik, D.E. Hibbs, M.B. Hursthouse, K.M.A. Malik, J. Chem. Soc. Perkin Trans. 2 (1997) 721.
[200] R.K. Harris, A. Nordon, K.D.M. Harris, Magn. Reson. Chem. 37 (1999) 15.
[201] L. Olivier, R. Poupko, H. Zimmermann, Z. Luz, J. Phys. Chem. 100 (1996) 17995.
[202] R. Poupko, H. Zimmermann, K. Muller, Z. Luz, J. Am. Chem. Soc. 118 (1996) 7995.
[203] Z. Luz, R. Poupko, S. Alexander, J. Chem. Phys. 99 (1993) 7544.
[204] B.H. Meier, W.L. Earl, J. Am. Chem. Soc. 107 (1985) 5553.
[205] H. Günther, D. Moskau, P. Bast, D. Schmalz, Angew. Chem. Int. Ed. Engl. 26 (1987) 1212.
[206] J.D. Swalen, Prog. Nucl. Magn. Reson. Spectrosc. 1 (1966) 205.
[207] S. Castellano, A.A. Bothner-By, J. Chem. Phys. 41 (1964) 3863.
[208] R.B. Johannesen, J.A. Ferretti, R.K. Harris, J. Magn. Reson. 3 (1970) 84.
[209] A.R. Quirt, J.S. Martin, J. Magn. Reson. 5 (1971) 318.
[210] V. Lueg, G. Haegele, J. Magn. Reson. 26 (1977) 505.
[211] D. Massiot, F. Fayon, M. Capron, I. King, S. LeCalve, B. Alonso, J.O. Durand, B. Bujoli, Z. Gan, G.L. Hoatson, Magn. Reson. Chem. 40 (2002) 70.
[212] J. Higinbotham, I. Marshall, Annu. Rep. NMR Spectrosc. 43 (2001) 59.
[213] D.A. Kleier, G. Binsch, J. Magn. Reson. 3 (1970) 146.
[214] D.S. Stephenson, G. Binsch, J. Magn. Reson. 30 (1978) 625.
[215] E.W. Abel, T.P.J. Coston, K.G. Orrell, V. Sik, D. Stephenson, J. Magn. Reson. 70 (1986) 34.
[216] N.R. Draper, H. Smith, Applied Regression Analysis, Wiley, Toronto, 1981.
[217] G.A.F. Seber, C.J. Wild, Nonlinear Regression, Wiley, New York, 1989.
[218] W.H. Press, B.P. Flannery, S.A. Teukolsky, W.T. Vetterling, Numerical Recipes in C. The Art of Scientific Computing, Cambridge University Press, Cambridge, 1988.
[219] J.A. Nelder, R. Mead, Comput. J. 7 (1965) 308.
[220] R.C. Ferguson, D.W. Marquardt, J. Chem. Phys. 41 (1964) 2087.
[221] T.K. Liepert, D.W. Marquardt, J. Magn. Reson. 24 (1976) 181.
[222] A.D. Bain, D.M. Rex, R.N. Smith, Magn. Reson. Chem. 39 (2001) 122.
[223] G.E. Hawkes, K.D. Sales, L.Y. Lian, R. Gobetto, Proc. R. Soc. London A 424 (1989) 93.
[224] P. Yip, D.A. Case, J. Magn. Reson. 83 (1989) 643.
[225] T. Fauconnier, C.J.L. Lock, R.A. Bell, J.F. Britten, K. Rainsford, Can. J. Chem. 72 (1994) 382.